

Zero-current Nonequilibrium State in Symmetric Exclusion Process with Dichotomous Stochastic Resetting

Onkar Sadekar

Indian Institute of Science Education and Research,
Homi Bhabha Road, Pashan, Pune 411008, India

Urna Basu

Raman Research Institute,
C. V. Raman Avenue, Bengaluru 560080, India

Abstract.

We study the dynamics of symmetric exclusion process (SEP) in the presence of stochastic resetting to two possible specific configurations — with rate r_1 (respectively, r_2) the system is reset to a step-like configuration where all the particles are clustered in the left (respectively, right) half of the system. We show that this dichotomous resetting leads to a range of rich behaviour, both dynamical and in the stationary state. We calculate the exact stationary profile in the presence of this dichotomous resetting and show that the diffusive current grows linearly in time, but unlike the resetting to a single configuration, the current can have negative average value in this case. For $r_1 = r_2$, the average current vanishes, and density profile becomes flat in the stationary state, similar to the equilibrium SEP. However, the system remains far from equilibrium and we characterize the nonequilibrium signatures of this ‘zero-current state’. We show that both the spatial and temporal density correlations in this zero-current state are radically different than in equilibrium SEP. We also study the behaviour of this zero-current state under an external perturbation and demonstrate that its response differs drastically from that of equilibrium SEP - while a small driving field generates a current which grows as \sqrt{t} in the absence of resetting, the zero-current state in the presence of dichotomous resetting shows a current $\sim t$ under the same perturbation.

1. Introduction

Introduction of stochastic resetting changes the statistical properties of a system drastically. Recent years have seen a tremendous surge in studying the effect of resetting on a wide variety of systems [1]. The paradigmatic example is that of a Brownian particle whose position is stochastically reset to a fixed point in space [2, 3, 4]. This results in a set of intriguing behavior like non-trivial stationary distribution, unusual dynamical relaxation behaviour and a finite mean first-passage time. Various generalizations and extensions of this model have been studied [5, 6, 7, 8, 9, 10]; resetting in the presence of an external potential or confinement [11, 12, 13, 14], resetting of an underdamped particle [15] and resetting to already excursed positions [16, 17, 18] are some notable examples. Moreover, instead of a constant resetting rate, other resetting protocols have also been studied which lead to a wide range of novel statistical properties. Examples include space [19] and time-dependent resetting rates [20, 21], non-Markovian resetting [22, 23, 24], resetting followed by a refractory period [25, 26] and resetting with space-time coupled return protocols [27].

An important issue which has gained a lot of attention recently is the effect of resetting on extended systems with many interacting degrees of freedom. This question has been studied in the context of fluctuating surfaces [28], coagulation-diffusion processes [29], symmetric exclusion process [30], zero-range process and its variants [31, 32] and Ising model [33]. It has been shown that introduction of resetting leads to a wide range of novel phenomena in these systems. A particularly interesting question is how the presence of resetting affects the behaviour of current, which plays an important role in characterizing nonequilibrium stationary states of such extended systems. The exclusion processes [34, 35], which refer to a class of simple and well studied models of interacting particles, are particularly suitable candidates for exploring these issues. It has been shown recently that for the simple symmetric exclusion process, the presence of stochastic resetting drastically affects the behaviour of the current [30]. A natural question is what happens to the current if more complex resetting protocols are used. A first step is to study a scenario with more than one resetting rates which take the system to different configurations.

In this article we address this question with a dichotomous resetting protocol in the context of Symmetric Exclusion Process (SEP). We study the behaviour of SEP in the presence of stochastic resetting to either of two specific configurations with different rates r_1 and r_2 . The two resetting configurations are chosen to be two complementary step-like configurations where all the particles are concentrated in the left-half, respectively, right-half, of the system. We calculate the exact time-dependent and stationary density profile in the presence of this dichotomous resetting. We also investigate the behaviour of the diffusive current and show that, similar to the case with resetting to one configuration, in the long-time regime the current grows linearly with time. However, depending on whether r_1 is larger than r_2 or not, the average current can be positive or negative. Moreover, it turns out that, in the short-time regime, a

superlinear temporal growth $\sim t^{3/2}$ of the average current can be observed depending on the choice of the initial condition. We also calculate the variance, skewness and kurtosis of the current distribution for small values of the resetting rates $r_1, r_2 \ll 1$, and show that, in the long time limit, the fluctuations of the diffusive current are characterized by a Gaussian distribution.

For the special case $r_1 = r_2$, the stationary profile becomes flat and the diffusive particle current vanishes. We explore the question - how is this zero-current state (ZCS) different than equilibrium SEP? To answer this question, we explore the nature of the spatial and temporal correlations in the ZCS. It turns out that, the presence of resetting has a strong effect on both the spatial and temporal correlations of the system. We show that, even though flat, the density profile is strongly correlated, contrary to the equilibrium case. On the other hand, the temporal auto-correlation in ZCS decays exponentially with time, as opposed to an algebraic decay in equilibrium. Moreover, we study the effect of an external perturbation on this state by adding an external drive along the central bond which biases the hopping rate across the bond. We show that the response of the ZCS is drastically different than that of ordinary SEP - while the current generated due to the perturbation grows as $\sim \sqrt{t}$ for equilibrium SEP, in the presence of the dichotomous resetting, the same perturbation leads to a linear temporal growth in the diffusive current.

The structure of the paper is as follows. In the next Section we define the dynamics of simple exclusion process with dichotomous resetting and derive the corresponding renewal equation. The dynamical and stationary behaviour of the density profile is investigated in Sec. 3. In Sec. 4 we study the behaviour of the diffusive current including its moments and distribution. Sec. 5 is devoted to the study of the special scenario $r_1 = r_2$: How current fluctuations and configurations weights in ZCS differ from SEP is discussed in Sec. 5.1 and 5.2. In Sec. 5.3 and 5.4 we explore the behaviour of the spatial and temporal correlation of the density. The response of the system to an external perturbation is investigated in Sec. 5.5. We conclude with a summary of our results in Sec. 6.

2. Model

Let us consider a periodic lattice of size L where each site x can either be occupied by one particle or be vacant; correspondingly, the site variable $s_x = 1, 0$. Consequently, the configuration \mathcal{C} of the system is characterized by an array $\mathcal{C} = \{s_x; x = 0, 1, \dots, L-1\}$. Moreover, we consider the case of half-filling, *i.e.*, the number of particles $\sum_x s_x = L/2$. The configuration evolves following two different kinds of dynamical moves, namely, hopping and resetting. The hopping dynamics is the usual one for ordinary symmetric exclusion process - a randomly chosen particle hops to one of its neighbouring sites with unit rate, provided the target site is empty. The stochastic resetting dynamics refers to an abrupt change in the configuration - at any time, the system is ‘reset’ to either of the two specific configurations \mathcal{C}_1 and \mathcal{C}_2 , with rates r_1 and r_2 , respectively. In this

work we choose \mathcal{C}_1 and \mathcal{C}_2 to be two step-like configurations where all the particles are clustered in the left, respectively right, half of the system, *i.e.*,

$$\mathcal{C}_1 = \begin{cases} s_x = 1 & 0 \leq x \leq \frac{L}{2} - 1 \\ s_x = 0 & \text{otherwise} \end{cases}, \quad \text{and} \quad \mathcal{C}_2 = \begin{cases} s_x = 0 & 0 \leq x \leq \frac{L}{2} - 1 \\ s_x = 1 & \text{otherwise} \end{cases}. \quad (1)$$

This stochastic resetting to either of the two complimentary configurations with different rates is referred to as ‘dichotomous resetting’ in the rest of the paper. The behaviour of SEP with resetting to only one possible configuration was studied in Ref. [30]. In this work we will show that in the presence of dichotomous resetting the system shows a much more rich behaviour including an interesting nonequilibrium zero-current stationary state, whose properties we will characterize.

Let $\mathcal{P}(\mathcal{C}, t | \mathcal{C}_0, 0)$ denote the probability that the configuration of the system is \mathcal{C} at time t , starting from some initial configuration \mathcal{C}_0 at time $t = 0$. The master equation governing the evolution of $\mathcal{P}(\mathcal{C}, t | \mathcal{C}_0, 0)$ reads,

$$\frac{d}{dt} \mathcal{P}(\mathcal{C}, t | \mathcal{C}_0, 0) = \mathcal{L}_0 \mathcal{P}(\mathcal{C}, t | \mathcal{C}_0, 0) - (r_1 + r_2) \mathcal{P}(\mathcal{C}, t | \mathcal{C}_0, 0) + r_1 \delta_{\mathcal{C}, \mathcal{C}_1} + r_2 \delta_{\mathcal{C}, \mathcal{C}_2}, \quad (2)$$

where \mathcal{L}_0 denotes the Markov Matrix in the absence of resetting. In other words, $\mathcal{L}_0 \mathcal{P}(\mathcal{C}, t) = \sum_{\mathcal{C}'} [W_{\mathcal{C}' \rightarrow \mathcal{C}} \mathcal{P}(\mathcal{C}', t) - W_{\mathcal{C} \rightarrow \mathcal{C}'} \mathcal{P}(\mathcal{C}, t)]$ where $W_{\mathcal{C}' \rightarrow \mathcal{C}}$ represents the jump rate from configuration \mathcal{C}' to \mathcal{C} due to hopping dynamics only. This rate is equal to 1 only if \mathcal{C} can be obtained from \mathcal{C}' by a single hop of a particle to either of its vacant neighbouring sites. Equation (2) can be formally solved to get,

$$\mathcal{P}(\mathcal{C}, t | \mathcal{C}_0, 0) = e^{(\mathcal{L}_0 - r)t} \delta_{\mathcal{C}, \mathcal{C}_0} + r_1 \int_0^t ds e^{(\mathcal{L}_0 - r)s} \delta_{\mathcal{C}, \mathcal{C}_1} + r_2 \int_0^t ds e^{(\mathcal{L}_0 - r)s} \delta_{\mathcal{C}, \mathcal{C}_2}, \quad (3)$$

where $r = r_1 + r_2$ denotes the sum of the two resetting rates. Now, let us note that $e^{\mathcal{L}_0 t} \delta_{\mathcal{C}, \mathcal{C}_i}$ is nothing but $\mathcal{P}_0(\mathcal{C}, t | \mathcal{C}_i, 0)$ – probability that the configuration is \mathcal{C} at time t , starting from some configuration \mathcal{C}_i , *in the absence of resetting*. Equation (3) then can be rewritten as,

$$\begin{aligned} \mathcal{P}(\mathcal{C}, t | \mathcal{C}_0, 0) &= e^{-rt} \mathcal{P}_0(\mathcal{C}, t | \mathcal{C}_0, 0) + r_1 \int_0^t ds e^{-rs} \mathcal{P}_0(\mathcal{C}, s | \mathcal{C}_1, 0) + r_2 \int_0^t ds e^{-rs} \mathcal{P}_0(\mathcal{C}, s | \mathcal{C}_2, 0) \\ &= e^{-rt} \mathcal{P}_0(\mathcal{C}, t | \mathcal{C}_0, 0) + r \int_0^t ds e^{-rs} [\alpha \mathcal{P}_0(\mathcal{C}, s | \mathcal{C}_1, 0) + (1 - \alpha) \mathcal{P}_0(\mathcal{C}, s | \mathcal{C}_2, 0)], \end{aligned} \quad (4)$$

where, in the last step, we have used $\alpha = \frac{r_1}{r_1 + r_2}$.

Equation (4) is nothing but the renewal equation for the dichotomous resetting, which can be understood easily using arguments similar to those used for single resetting configuration [2, 28]. Let us consider the system at some time t and let s be the time elapsed since the last resetting event. Now, the probability that no resetting event occurred during this interval is given by re^{-rs} (let us recall that $r = r_1 + r_2$) where $0 \leq s \leq t$ is a random variable. During the interval $[t - s, t]$ the system evolves following ordinary SEP dynamics, starting from \mathcal{C}_1 , or \mathcal{C}_2 , depending on the last resetting configuration. Now, probability that the last resetting was to configuration \mathcal{C}_1 , respectively \mathcal{C}_2 , is nothing but $\alpha = \frac{r_1}{r}$, respectively $1 - \alpha = \frac{r_2}{r}$. Then, the probability that the system is at configuration \mathcal{C} at time t with at least one resetting event occurring

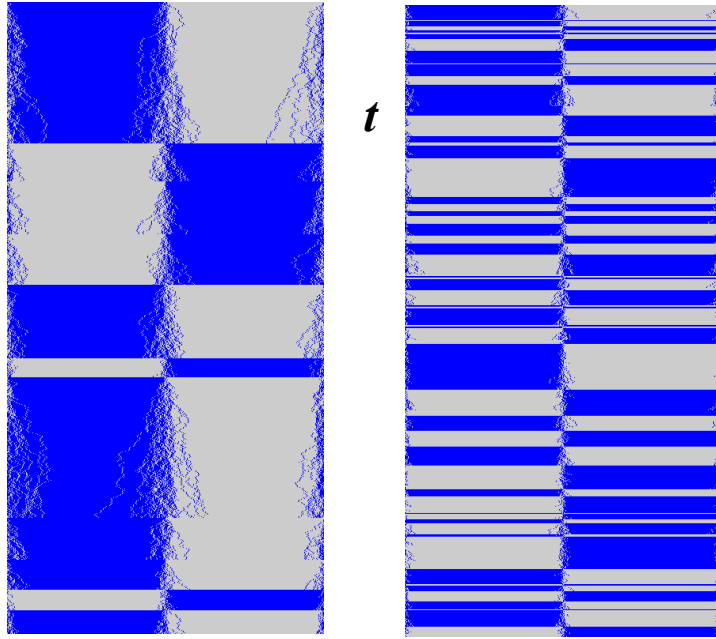


Figure 1. Typical snapshots for the SEP with dichotomous resetting for a system of size $L = 400$. The left panel shows the time-evolution for $r_1 = r_2 = 0.005$ and the right panel shows the same for $r_1 = r_2 = 0.05$.

during $[0, t]$ is given by the integral in Eq. (4). The first term corresponds to the scenario where no resetting event occurred during time t (probability e^{-rt}) and the system evolved as ordinary SEP during the whole time.

The typical time duration between two consecutive resetting events is r^{-1} , irrespective of which configuration it resets to. As mentioned above, during this time the system evolves following the hopping dynamics only. Figure (1) shows typical time-evolution of the system for two different values of r , with $r_1 = r_2$. In the following we study the behavior of SEP in the presence of dichotomous resetting.

3. Density profile

In this section, we investigate the dynamical and static behaviour of the density profile $\rho(x, t) = \langle s_x(t) \rangle$ in the presence of the dichotomous resetting. For resetting to only one configuration the exact time-evolution of the density profile has been calculated in Ref. [30]. Here we follow the same procedure to investigate the behaviour of the density profile for the dichotomous case.

The time evolution equation for $\rho(x, t)$ can be obtained by multiplying Eq. (2) by s_x and then summing over all possible configurations \mathcal{C} ,

$$\frac{d}{dt}\rho(x, t) = \rho(x+1, t) + \rho(x-1, t) - 2\rho(x, t) - r\rho(x, t) + r_1\phi_1(x) + r_2\phi_2(x). \quad (5)$$

Here, $\phi_1(x)$ and $\phi_2(x)$ are the density profiles corresponding to the resetting configurations \mathcal{C}_1 and \mathcal{C}_2 respectively. Equation (5) can be solved using the Fourier

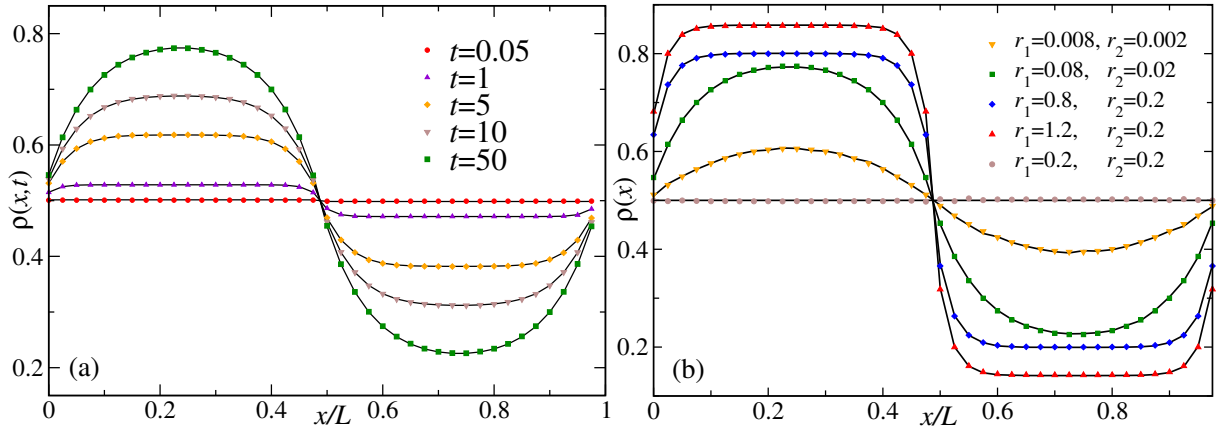


Figure 2. Density profile: (a) Evolution of $\rho(x, t)$ as a function of time t for $r_1 = 0.08$ and $r_2 = 0.02$. (b) Plot of the stationary profile $\rho(x)$ as a function of x/L for different values of r_1 and r_2 . The solid lines correspond to the analytical results whereas the symbols correspond to the data obtained from numerical simulations. The system size $L = 40$ here.

transform of $\rho(x, t)$,

$$\tilde{\rho}(n, t) = \sum_{x=0}^{L-1} e^{i \frac{2\pi n x}{L}} \rho(x, t) \quad \text{with } n = 0, 1, 2, \dots, L-1. \quad (6)$$

Substituting Eq. (6) in Eq. (5) we get,

$$\frac{d}{dt} \tilde{\rho}(n, t) = -(\lambda_n + r) \tilde{\rho}(n, t) + r_1 \tilde{\phi}_1(n) + r_2 \tilde{\phi}_2(n), \quad (7)$$

where $\lambda_n = 2(1 - \cos \frac{2\pi n}{L})$ and $\tilde{\phi}_1(n)$ and $\tilde{\phi}_2(n)$ are the Fourier transforms of $\phi_1(x)$ and $\phi_2(x)$ respectively. Eq. (7) can be solved immediately to obtain,

$$\tilde{\rho}(n, t) = \left[\tilde{\phi}_0(n) - \frac{r_1 \tilde{\phi}_1(n) + r_2 \tilde{\phi}_2(n)}{\lambda_n + r} \right] e^{-(\lambda_n + r)t} + \frac{r_1 \tilde{\phi}_1(n) + r_2 \tilde{\phi}_2(n)}{\lambda_n + r}. \quad (8)$$

Here, $\tilde{\phi}_0(n)$ denotes the Fourier transform of initial density profile $\rho(x, 0)$. We can obtain $\rho(x, t)$ from Eq. (8) by taking the inverse Fourier transform of $\tilde{\rho}(n, t)$,

$$\rho(x, t) = \frac{1}{L} \sum_{n=0}^{L-1} \left[\tilde{\phi}_0(n) e^{-(\lambda_n + r)t} + \frac{r_1 \tilde{\phi}_1(n) + r_2 \tilde{\phi}_2(n)}{\lambda_n + r} (1 - e^{-(\lambda_n + r)t}) \right] e^{-i \frac{2\pi n x}{L}}. \quad (9)$$

It is to be noted that $\rho(x, t)$ also satisfies a renewal equation which can easily be derived from Eq. (4),

$$\rho(x, t) = e^{-rt} \rho_0^0(x, t) + r \int_0^t ds e^{-rs} [\alpha \rho_0^1(x, t) + (1 - \alpha) \rho_0^2(x, t)]. \quad (10)$$

Here $\rho_0^i(x, t)$ denotes the density at time t , starting from the initial profile $\phi_i(x)$, for ordinary SEP (the subscript 0 refers to the absence of resetting). Recalling that, $\rho_0^i(x, t) = \frac{1}{L} \sum_{n=0}^{L-1} e^{-i \frac{2\pi n x}{L}} e^{-\lambda_n t} \tilde{\phi}_i(n)$ (see Ref [30]), it is straightforward to show that Eq. (10) is equivalent to Eq. (9).

To proceed further we need to specify the initial condition. Let us consider the case where initially the system starts from \mathcal{C}_1 and \mathcal{C}_2 with equal probability. In that case, $\rho(x, 0) = \phi_0(x) = \frac{1}{2}[\phi_1(x) + \phi_2(x)]$. For our specific choice of $\mathcal{C}_{1,2}$ (see Eq. (1)) we have $\phi_1(x) = \Theta(\frac{L}{2} - 1 - x)$ and $\phi_2(x) = \Theta(x - \frac{L}{2})$ where the Heaviside Theta function is defined as $\Theta(x) = 1$ for $x \geq 0$ and it is zero elsewhere. Consequently, $\phi_1(x) + \phi_2(x) = 1 \forall x$ and we have $\tilde{\phi}_0(n) = \frac{L}{2}\delta_{n0}$. Additionally, we also have, $\tilde{\phi}_i(0) = \frac{L}{2}$, $i = 1, 2$. For $n \neq 0$, $\tilde{\phi}_2(n) = -\tilde{\phi}_1(n)$. It is easy to see that (see Ref. [30]),

$$\tilde{\phi}_1(n) = \begin{cases} 1 + i \cot \frac{\pi n}{L} & \text{for } n = 1, 3, 5, \dots \\ 0 & \text{for even } n \geq 2. \end{cases} \quad (11)$$

Substituting the above results in Eq. (9) and simplifying we get,

$$\rho(x, t) = \frac{1}{2} + \frac{1}{L} \left[\sum_{n=1,3}^{L-1} \left(\frac{r_1 - r_2}{\lambda_n + r_1 + r_2} \right) \left(1 + i \cot \frac{\pi n}{L} \right) e^{-i \frac{2\pi n x}{L}} (1 - e^{-(\lambda_n + r)t}) \right]. \quad (12)$$

Note that, for any value of x and t , $\rho(x, t; r_1, r_2) = \frac{1}{2} - \rho(x, t; r_2, r_1)$. For this reason, it suffices to study only the regime $r_1 \geq r_2$. Figure 2(a) shows the time-evolution of $\rho(x, t)$ for $r_1 = 0.08$ and $r_2 = 0.02$; starting from a flat profile at time $t = 0$, where the density at each site equals $\frac{1}{2}$, the average density profile evolves to a non-trivial inhomogeneous stationary state. The stationary profile can be obtained by taking the $t \rightarrow \infty$ limit in Eq. (12) and yields,

$$\rho(x) = \frac{1}{2} + \frac{1}{L} \left[\sum_{n=1,3}^{L-1} \left(\frac{r_1 - r_2}{\lambda_n + r} \right) \left(1 + i \cot \frac{\pi n}{L} \right) e^{-i \frac{2\pi n x}{L}} \right]. \quad (13)$$

Figure 2(b) shows plots of $\rho(x)$ for a set of different values of (r_1, r_2) .

A special situation arises when the two resetting rates are equal, *i.e.*, $r_1 = r_2 = \frac{r}{2}$. In this case, as can be seen from Eq. (13), the stationary profile remains flat irrespective of the value of r .[‡] This is reminiscent of the ordinary SEP in equilibrium. However, in the presence of the dichotomous resetting, the system remains far away from equilibrium although it is not apparent from the density profile alone. We will come back to this question later in Sec. 5.

4. Diffusive Current

In the absence of resetting, starting from either of the two step-like configurations \mathcal{C}_1 and \mathcal{C}_2 , the hopping of particles results in a diffusive particle current. Quantified by the net number of particles crossing the central bond up to time t , this diffusive current increases $\sim \sqrt{t}$ for a thermodynamically large system [36, 37]. It has been shown that the presence of stochastic resetting to only one configuration, namely \mathcal{C}_1 , alters the behaviour of the diffusive current drastically, resulting in a linear growth in time [30]. In that case, because of the choice of the resetting configuration, the net motion of the particles always remains from the left to the right-half of the system. The presence of

[‡] In fact, for our specific choice of initial condition, for $r_1 = r_2$, $\rho(x, t) = \frac{1}{2}$ at all times $t \geq 0$.

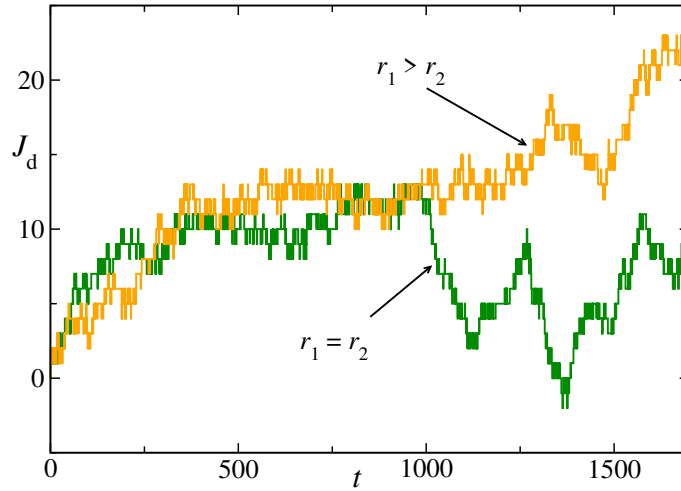


Figure 3. Two typical trajectories for J_d for $r_1 = r_2$ and $r_1 > r_2$ respectively. Note that the trajectory for $r_1 < r_2$ would be qualitatively same as the $r_1 > r_2$ case except for overall decrease instead of increase in J_d .

the dichotomous resetting can change that, as resetting to C_2 would give rise to particles moving to the left-half from the right-half of the system. Figure 3 shows a plot of the diffusive current J_d along a couple of typical trajectories for r_1 larger than and equal to r_2 ; the sudden increase (decrease) in J_d indicates a resetting to C_1 (C_2). In this section we quantitatively characterize the behaviour of the diffusive current in the presence of dichotomous resetting, for arbitrary values of r_1, r_2 .

The instantaneous diffusive current $j_d(t)$ at time t is defined as the net number of particles crossing the central bond $(\frac{L}{2} - 1, \frac{L}{2})$ from left to right, in the time interval $(t, t + dt)$. The average instantaneous current, then, is nothing but the density gradient across the central bond,

$$\langle j_d(t) \rangle = \left\langle s_{\frac{L}{2}-1} \left(1 - s_{\frac{L}{2}} \right) \right\rangle - \left\langle s_{\frac{L}{2}} \left(1 - s_{\frac{L}{2}-1} \right) \right\rangle = \rho \left(\frac{L}{2} - 1, t \right) - \rho \left(\frac{L}{2}, t \right). \quad (14)$$

Using the expression for $\rho(x, t)$ from Eq. (12) in Eq. (14) we get,

$$\langle j_d(t) \rangle = \frac{2(r_1 - r_2)}{L} \sum_{n=1,3}^{L-1} \frac{1 - e^{-(\lambda_n + r)t}}{\lambda_n + r}. \quad (15)$$

Clearly, the average instantaneous current becomes negative when $r_1 < r_2$.

We are interested in the behaviour of the total time-integrated current $J_d(t)$ which measures the total number of particles crossing the central bond up to time t . The average total current $\langle J_d(t) \rangle$ can be obtained by integrating the average instantaneous current $\langle J_d(t) \rangle = \int_0^t dt' \langle j_d(t') \rangle$. Integrating Eq. (15) we get,

$$\langle J_d(t) \rangle = \frac{2(r_1 - r_2)}{L} \sum_{n=1,3}^{L-1} \left[\frac{t}{\lambda_n + r} - \frac{(1 - e^{-(\lambda_n + r)t})}{(\lambda_n + r)^2} \right]. \quad (16)$$

For thermodynamically large system, *i.e.*, $L \rightarrow \infty$, the sum in the above equation can

be converted to an integral over $q = \frac{2\pi n}{L}$, and yields,

$$\begin{aligned}\langle J_d(t) \rangle &= (r_1 - r_2) \int_0^{2\pi} \frac{dq}{2\pi} \left[\frac{t}{\lambda_q + r} - \frac{(1 - e^{-(\lambda_q + r)t})}{(\lambda_q + r)^2} \right] \\ &= (r_1 - r_2) \left[\frac{t}{\sqrt{r(4+r)}} - \frac{(2+r)}{r(4+r)} + \int_0^{2\pi} \frac{dq}{2\pi} \frac{e^{-(\lambda_q + r)t}}{(\lambda_q + r)^2} \right].\end{aligned}\quad (17)$$

In the long time regime, the exponential term decays and we have a linear temporal growth of the diffusive current,

$$\langle J_d(t) \rangle = \frac{(r_1 - r_2)t}{\sqrt{r(4+r)}} = (2\alpha - 1) \sqrt{\frac{r}{4+r}} t. \quad (18)$$

It is to be noted that the above expression has a very similar form to the long-time average current in case of single resetting (see Eq. (23) in Ref [30]); the dependence on the total resetting rate r is the same in both the cases, but a prefactor $(r_1 - r_2)$ arises in the presence of dichotomous resetting which allows the average current to become negative if $r_2 > r_1$. For the special case when $r_1 = r_2$, $\langle J_d(t) \rangle$ vanishes. This feature is unique to dichotomous resetting and we will discuss it in more details in a later Section.

It is also interesting to investigate the short-time behaviour of the average current. Equation (17) provides an exact expression which is valid at all times and can be used to compute $\langle J_d(t) \rangle$ by performing the q -integral numerically. However, an alternative form for $\langle J_d(t) \rangle$, which lends itself more easily to numerical evaluation, can be derived using the renewal Equation (10) for $\rho(x, t)$. Since the average instantaneous current $\langle j_d(s) \rangle$ is the gradient of density across the central bond, we have a similar renewal equation for it,

$$\langle j_d(s) \rangle = (r_1 - r_2) \int_0^s ds' \langle j_0^1(s') \rangle, \quad (19)$$

where $\langle j_0^1(s) \rangle$ denotes the average instantaneous current in the absence of resetting, starting from the configuration \mathcal{C}_1 . § Note that, there is no contribution from the initial condition as we have chosen the initial profile to be completely flat. The average instantaneous current $\langle j_0^1(s) \rangle$ is known exactly in terms of the Modified Bessel function of the first kind: $\langle j_0^1(s) \rangle = e^{-2s} I_0(2s)$ [30]. The average total current is then obtained by integrating Eq. (19),

$$\begin{aligned}\langle J_d(t) \rangle &= (r_1 - r_2) \int_0^t ds \int_0^s ds' e^{-(r+2)s'} I_0(2s') \\ &= (r_1 - r_2) \int_0^t ds (t-s) e^{-(r+2)s} I_0(2s).\end{aligned}\quad (20)$$

$\langle J_d(t) \rangle$ at any time t can be obtained by numerically evaluating the integral in the above equation; it can also be shown easily that Eq. (20) is equivalent to Eq. (17). Also, note that $\langle J_d(r_1, r_2) \rangle = -\langle J_d(r_2, r_1) \rangle$ at all times t , hence it suffices to look at $\langle J_d(t) \rangle$ for $r_1 > r_2$ only. Figure 4(a) shows plots of $\langle J_d(t) \rangle$ obtained from Eq. (20) for a set of

§ The superscript 1 indicates the initial configuration \mathcal{C}_1 and the subscript 0 indicates the absence of resetting. We will use this convention again later.

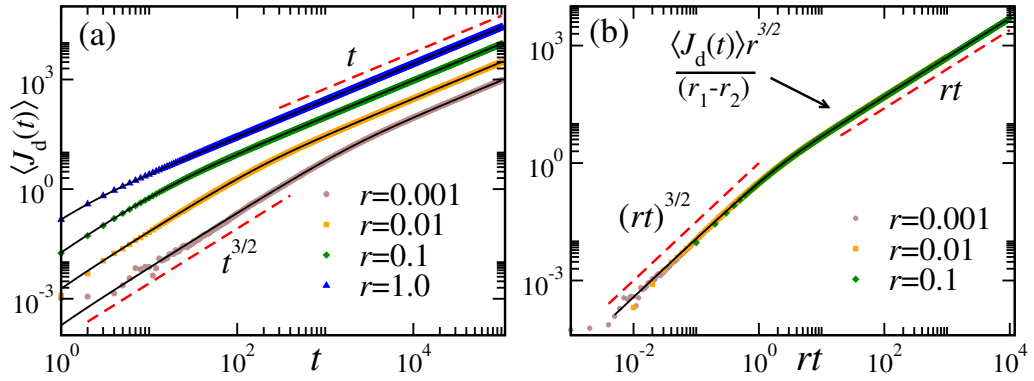


Figure 4. Diffusive current: (a) Plot of $\langle J_d(t) \rangle$ as a function of time t for different values of r and $\alpha = 0.8$. The solid lines correspond to the exact results (see Eqs. (17) and (18)) and the symbols correspond to the data obtained from numerical simulations. (b) Scaling collapse of the data in (a) according to Eq. (22). The solid line corresponds to the scaling function in Eq. (22). The numerical simulation is done on a lattice of size $L = 1000$ and averaged over more than 10^7 trajectories.

values of r (solid lines) for a fixed α , along with the same obtained from numerical simulations (symbols); a perfect agreement between the two sets verifies our analytical prediction.

Equation (20) can be used to derive an explicit expression for $\langle J_d(t) \rangle$ for small values of $r \ll 1$. In this case, the integrand is dominated by the large values of $s \gg r^{-1}$. Using the asymptotic behaviour of $I_0(2x)$ for large x (see Ref. [38], Eq. 10.40.1) and a variable transformation $u = rs$, we get,

$$\langle J_d(t) \rangle \simeq \frac{(r_1 - r_2)}{2\sqrt{\pi}r^3} \int_0^{rt} du \frac{(rt - u)}{\sqrt{u}} e^{-u}. \quad (21)$$

The above integral can be computed exactly, and yields,

$$\langle J_d(t) \rangle \simeq \frac{(r_1 - r_2)}{\sqrt{r^3}} \left[\frac{e^{-rt}\sqrt{rt}}{2\sqrt{\pi}} + \frac{1}{4}(2rt - 1) \operatorname{erf}(\sqrt{rt}) \right]. \quad (22)$$

Clearly, for large time $t \gg r^{-1}$, the above equation predicts $\langle J_d \rangle \simeq (r_1 - r_2)t/2\sqrt{r}$, which is consistent with Eq. (18) in the small r limit. One can also extract the short-time behaviour of the average current from Eq. (22) and it turns out that for $t \ll r^{-1}$, the average current shows a super-linear growth,

$$\langle J_d(t) \rangle \simeq \frac{3(r_1 - r_2)}{2\sqrt{\pi}} t^{3/2} + \mathcal{O}(t^{5/2}). \quad (23)$$

It should be emphasized that the short-time behaviour depends on the specific initial condition considered. Depending on the choice of initial configuration, the current can show very different short-time behaviour — it is easy to see that, while starting with \mathcal{C}_1 and \mathcal{C}_2 with equal probabilities leads to the $t^{3/2}$ growth, starting with \mathcal{C}_1 only leads to a $\sim \sqrt{t}$ behaviour.

We will conclude the discussion about the average diffusive current with one final comment. From Eq. (22), it appears that $\langle J_d(t) \rangle r^{3/2}/(r_1 - r_2)$ depends only on rt , and

not on r_1, r_2 separately. Figure 4(b) shows a plot of $\langle J_d(t) \rangle r^{3/2} / (r_1 - r_2)$ as a function of rt for different small values of r ; the collapsed curve is compared with the scaling function predicted by Eq. (22) (solid line).

Fluctuations of J_d : To characterize the behaviour of the diffusive current, it is also important to understand the nature of its fluctuations. To this end, we investigate the higher moments of J_d , starting with its variance. We use the method introduced in Ref. [30] and note that the net diffusive current along any trajectory in the duration $[0, t]$ can be written as a sum of the currents in the intervals between consecutive resetting events. Let us assume that there are n resetting events (irrespective of the configuration to which the system is reset) during the interval $[0, t]$ and let t_i denote the interval between the $(i - 1)^{th}$ and i^{th} events. The probability of such a trajectory is given by,

$$\mathcal{P}_n(\{t_i\}) = r^n e^{-r \sum_{i=1}^{n+1} t_i}, \quad (24)$$

where $t = \sum_{i=1}^{n+1} t_i$. Here, t_1 is the time before the first resetting event and t_{n+1} denotes the time between the last resetting and final time t . Along this trajectory, the total diffusive current is,

$$J_d = \sum_{i=1}^{n+1} J_0(t_i), \quad (25)$$

where $J_0(t_i)$ denotes the net hopping current during the interval t_i , in the absence of resetting, but starting from \mathcal{C}_1 , or \mathcal{C}_2 , depending on the $(i - 1)^{th}$ resetting event. Let us recall that, the resetting to \mathcal{C}_1 , respectively \mathcal{C}_2 , occurs with probability $\alpha = \frac{r_1}{r_1 + r_2}$, respectively $1 - \alpha = \frac{r_2}{r_1 + r_2}$. Then, the probability that the value of the diffusive current is $J_i \equiv J_0(t_i)$ during an interval t_i is given by,

$$P(J_i, t_i) = \alpha P_0^1(J_i, t_i) + (1 - \alpha) P_0^2(J_i, t_i) \quad \text{for } 2 \leq i \leq n + 1, \quad (26)$$

where $P_0^1(J_0, \tau)$ (respectively, $P_0^2(J_0, \tau)$) denotes the probability that the diffusive current will have a value J_0 during the interval τ starting from \mathcal{C}_1 (respectively, \mathcal{C}_2) in the absence of resetting. However, before the first resetting event, *i.e.*, for the time interval $[0, t_1]$, we have,

$$P(J, t_1) = \frac{1}{2} [P_0^1(J, t_1) + P_0^2(J, t_1)],$$

as we start from \mathcal{C}_1 and \mathcal{C}_2 with equal probability.

We can now write the probability that, in the presence of dichotomous resetting, the total diffusive current has a values J_d at time t ,

$$P(J_d, t) = \sum_{n=0}^{\infty} \int_0^t \prod_{i=1}^{n+1} dt_i \mathcal{P}_n(\{t_i\}) \delta(t - \sum_{i=1}^{n+1} t_i) \int \prod_{i=1}^{n+1} dJ_i P(J_i, t_i) \delta(J_d - \sum_i J_i), \quad (27)$$

where we have used the fact that the hopping currents J_i in the intervals t_i are independent of each other. To circumvent the constraints presented by the δ -functions, it is convenient to work with the Laplace transform of the moment generating function

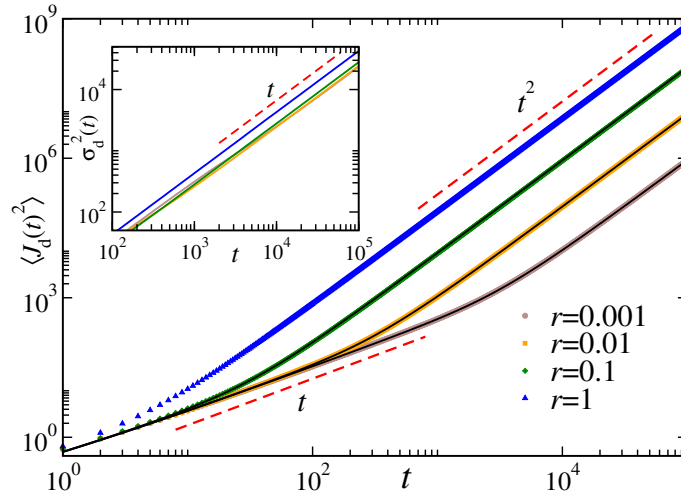


Figure 5. The second moment $\langle J_d(t)^2 \rangle$ of the diffusive current as a function of time t for different values of r and $\alpha_1 = 0.8$. The symbols correspond to the data obtained from numerical simulations and the black solid lines refer the analytical result for small r [see Eq. (39)]. The inset shows the corresponding plot for the variance $\sigma_d^2(t)$. The system size $L = 1000$ for the simulations.

$\langle e^{\lambda J_d} \rangle$ with respect to time,

$$Q(s, \lambda) = \mathcal{L}_{t \rightarrow s}[\langle e^{\lambda J_d} \rangle] = \int_0^\infty dt e^{-st} \int dJ_d e^{\lambda J_d} P(J_d, t). \quad (28)$$

Using Eq. (27) and performing the integrals over J_d and t , we get,

$$\begin{aligned} Q(s, \lambda) &= \sum_{n=0}^\infty r^n \int_0^\infty \prod_{i=1}^{n+1} dt_i e^{-(r+s)\sum_i t_i} \int \prod_{i=1}^{n+1} dJ_i e^{\lambda \sum_i J_i} P(J_i, t_i) \\ &= h_{\frac{1}{2}}(s, \lambda) \sum_{n=0}^\infty r^n h_\alpha(s, \lambda)^n, \end{aligned} \quad (29)$$

where,

$$h_\alpha(s, \lambda) = \int_0^\infty d\tau e^{-(r+s)\tau} \left[\alpha \int dJ_0 e^{\lambda J_0} P_0^1(J_0, \tau) + (1 - \alpha) \int dJ_0 e^{\lambda J_0} P_0^2(J_0, \tau) \right] \quad (30)$$

Now, let us recall that, the configurations \mathcal{C}_1 and \mathcal{C}_2 are complementary to each other — during some time interval τ , corresponding to each trajectory starting from \mathcal{C}_1 , with net current J_0 , there exists a trajectory starting from \mathcal{C}_2 , which yields net current $-J_0$. In other words, $P_0^2(J_0, \tau) = P_0^1(-J_0, \tau)$. Using this relation, Eq. (30) yields,

$$h_\alpha(s, \lambda) = \alpha h(s, \lambda) + (1 - \alpha) h(s, -\lambda), \quad (31)$$

where, for the sake of notational convenience, we have denoted,

$$h(s, \lambda) = \int_0^\infty d\tau e^{-(r+s)\tau} \int dJ_0 e^{\lambda J_0} P_0^1(J_0, \tau). \quad (32)$$

Using Eqs. (31) and (29), and performing the sum over n , we finally have,

$$Q(s, \lambda) = \frac{h(s, \lambda) + h(s, -\lambda)}{2[1 - r\{\alpha h(s, \lambda) + (1 - \alpha)h(s, -\lambda)\}]}. \quad (33)$$

To calculate $h(s, \lambda)$ exactly one needs $P_0^1(J_0, \tau)$, the current distribution in the absence of resetting, which, unfortunately, is not known for arbitrary values of τ . However, following the approach used in Ref. [30], we can compute $h(s, \lambda)$ for small values of r and s using the large-time moment generating function of $J_0(\tau)$, derived in Ref. [36]. In particular, for the initial configuration \mathcal{C}_1 it has been shown in Ref. [36, 30] that, for large values of τ ,

$$\int dJ_0 e^{\lambda J_0} P_0^1(J_0, \tau) \simeq e^{\sqrt{\tau} F(\lambda)}, \quad \text{with } F(\lambda) = -\frac{1}{\sqrt{\pi}} \text{Li}_{3/2}(1 - e^\lambda), \quad (34)$$

where $\text{Li}_\alpha(z)$ denotes the Poly-Logarithm function (see Ref. [38], Eq. 25.12.10).

Substituting Eq. (34) in Eq. (32) and evaluating the integral, we get, for small r, s ,

$$h(s, \lambda) \simeq \frac{1}{r+s} \left[1 + \frac{\sqrt{\pi} F(\lambda)}{2\sqrt{r+s}} e^{\frac{F(\lambda)^2}{4(r+s)}} \left(1 + \text{erf} \left[\frac{F(\lambda)}{2\sqrt{r+s}} \right] \right) \right]. \quad (35)$$

Now, we can extract the Laplace transform of any moment of J_d using Eq. (35) along with Eq. (33). First, we have,

$$\mathcal{L}_{t \rightarrow s}[\langle J_d(t) \rangle] = \frac{d}{d\lambda} Q(s, \lambda) \Big|_{\lambda=0} = \frac{r_1 - r_2}{2s^2 \sqrt{r+s}}. \quad (36)$$

The average current is obtained by taking the inverse Laplace transform,

$$\begin{aligned} \langle J_d(t) \rangle &= \mathcal{L}_{s \rightarrow t}^{-1} \left[\frac{r_1 - r_2}{2s^2 \sqrt{r+s}} \right] \\ &= \frac{(r_1 - r_2)}{\sqrt{r^3}} \left[\frac{e^{-rt} \sqrt{rt}}{2\sqrt{\pi}} + \frac{1}{4} (2rt - 1) \text{erf}(\sqrt{rt}) \right]. \end{aligned} \quad (37)$$

Note that, as expected, the above equation is identical to Eq. (22), which is also valid for small values of r and large t , albeit obtained using a different method.

Next, we calculate the second moment $\langle J_d(t)^2 \rangle$. The corresponding Laplace transform is obtained from Eq. (33),

$$\begin{aligned} \mathcal{L}_{t \rightarrow s}[\langle J_d^2(t) \rangle] &= \frac{d^2}{d\lambda^2} Q(s, \lambda) \Big|_{\lambda=0} \\ &= \frac{1}{\pi s^2} + \frac{(r_1 - r_2)^2}{2s^3 \sqrt{r+s}} + \frac{b\sqrt{r+s}}{2s^2}, \end{aligned} \quad (38)$$

where $b = 1 - \frac{1}{\sqrt{2}}$. Fortunately, we can invert the Laplace transform exactly to obtain the second moment of the diffusive current for small r and large values of t ,

$$\begin{aligned} \langle J_d^2(t) \rangle &= \frac{(r_1 - r_2)^2}{2r^3} + e^{-rt} \left[\frac{b}{2} \sqrt{\frac{t}{\pi}} - \frac{(r_1 - r_2)^2}{2r^3} \right] + t \left[\frac{1}{\pi} - \frac{(r_1 - r_2)^2}{2r^2} \right] \\ &\quad + \frac{(r_1 - r_2)^2 t^2}{4r} + \frac{b}{4\sqrt{r}} (1 + 2rt) \text{erf}(\sqrt{rt}). \end{aligned} \quad (39)$$

In the long-time limit $\langle J_d^2(t) \rangle$ shows a quadratic behaviour for any $r_1 \neq r_2$. The variance $\sigma_d^2 = \langle J_d^2(t) \rangle - \langle J_d(t) \rangle^2$ can be obtained using Eqs. (37) and (39). In particular, in the long-time limit, the variance increases linearly with time,

$$\sigma_d^2(t) \simeq t \left[\frac{1}{\pi} + \frac{\sqrt{r}}{2} \left(1 - \frac{1}{\sqrt{2}} \right) - \frac{(r_1 - r_2)^2}{4r^2} \right]. \quad (40)$$

Figure (5) shows a plot of $\langle J_d^2(t) \rangle$ vs time for a set of values of r . The inset shows the corresponding variance $\sigma_d^2(t)$ in the long-time regime.

To understand the nature of the fluctuation in more detail, next we explore the probability distribution $P(J_d, t)$. As noted in Eq. (25), the net diffusive current J_d is a sum of current $J_0(t_i)$ during intervals t_i between two consecutive resetting events. These $J_0(t_i)$ are completely independent of each other, and central limit theorem predicts that, when the number of resetting events is large, *i.e.*, for $rt \gg 1$, the typical distribution of the sum should be a Gaussian,

$$P(J_d, t) = \frac{1}{\sqrt{2\pi\sigma_d^2(t)}} \exp \left[-\frac{(J_d - \langle J_d(t) \rangle)^2}{2\sigma_d^2(t)} \right]. \quad (41)$$

It should be noted that, even for the case of resetting to a single configuration, the diffusive current shows a Gaussian behaviour in the long-time regime, although the mean and the variance are very different in that case. Figure (6) shows plots of $P(J_d, t)$ for different values of t which shows a very good agreement with the Gaussian (solid line) in the large time limit.

The argument used above to predict the Gaussian nature of $P(J_d, t)$ relies crucially on the central limit theorem, which holds true only when there are large number of resetting events, *i.e.*, $t \gg r^{-1}$. It is interesting to investigate how the distribution approaches the Gaussian limit. To understand this approach, we compute the skewness and the kurtosis of the distribution as a function of time. The skewness measures the ‘asymmetry’ in the distribution, and is defined as,

$$\gamma = \frac{\langle (J_d - \langle J_d \rangle)^3 \rangle}{\sigma_d^3} = \frac{\langle J_d^3 \rangle - 3\mu_d \sigma_d^2 - \mu_d^3}{\sigma_d^3}, \quad (42)$$

where we have used $\mu_d \equiv \langle J_d \rangle$ for notational brevity. A Gaussian distribution is symmetric around the mean and the skewness vanishes. A positive (negative) value of the skewness indicates a tail towards the right (left) side of the distribution. On the other hand, the kurtosis measures the ‘peakedness’ of a distribution and is defined as,

$$\kappa = \frac{\langle (J_d - \langle J_d \rangle)^4 \rangle}{\sigma_d^4} = \frac{\langle J_d^4 \rangle - 4\mu_d \langle J_d^3 \rangle + 6\mu_d^2 \sigma_d^2 + 3\mu_d^4}{\sigma_d^4}, \quad (43)$$

For a Gaussian distribution $\kappa = 3$; if $\kappa > 3$ it indicates a heavy-tailed distribution compared to a Gaussian one whereas $\kappa < 3$ indicates a more ‘peaked’ distribution.

To calculate γ and κ for $P(J_d, t)$ we need the third and fourth moments which can be calculated in a straightforward manner from Eq. (33). The Laplace transform of the third moment is given by,

$$\begin{aligned} \mathcal{L}_{t \rightarrow s}[\langle J_d^3(t) \rangle] &= \frac{d^3}{d\lambda^3} Q(s, \lambda) \Big|_{\lambda=0} \\ &= \frac{(r_1 - r_2)}{12\pi s^4 (r + s)^{3/2}} \left[9\pi \left((r_1 - r_2)^2 + brs(1 + 2s)(\sqrt{r + s}) \right) \right. \\ &\quad \left. 9s(4r + 3s + 4bs) - c_1 \pi s^2 (r + s) \right], \end{aligned} \quad (44)$$

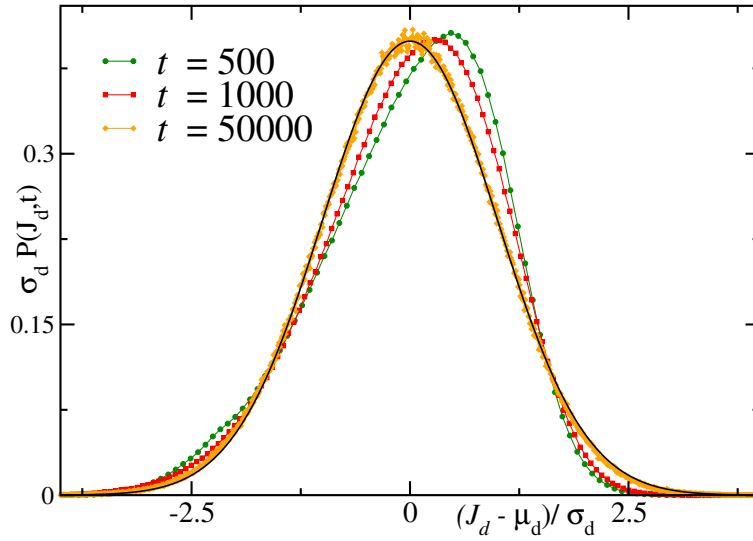


Figure 6. Probability distribution of the diffusive current. The symbols correspond to the data obtained from numerical simulations and the black solid line refers to the analytical result for large t [see Eq. (41)]. Here, $r_1 = 0.008$ and $\alpha_1 = 0.8$. The system size is $L = 1000$.

where $b = 1 - \frac{1}{\sqrt{2}}$ and $c_1 = -6 + 9\sqrt{2} - 4\sqrt{3}$. Similarly,

$$\begin{aligned} \mathcal{L}_{t \rightarrow s}[\langle J_d^4(t) \rangle] &= \frac{d^4}{d\lambda^4} Q(s, \lambda) \Big|_{\lambda=0} \\ &= \frac{3(r_1 - r_2)^4}{2s^5(r+s)^2} + \frac{3(r_1 - r_2)^2}{2\pi s^4(r+s)^2} \left[2(3r+2s) + b\sqrt{r+s}((8+\pi)s + 3\pi r) \right] \\ &\quad + \frac{1}{3\pi^2 s^3(r+s)} [6(3r+s) - c_1\pi^2(r_1 - r_2)^2] + \frac{3b(4r+3s)}{2\pi s^3\sqrt{r+s}} \\ &\quad - \frac{1}{12s^3} [3\pi c_2 s\sqrt{r+s} + 8c_1 s - 18b^2(\pi r + 2s)], \end{aligned} \quad (45)$$

where, as before, $b = 1 - \frac{1}{\sqrt{2}}$ and $c_1 = -6 + 9\sqrt{2} - 4\sqrt{3}$, $c_2 = 4 + 7\sqrt{2} - 8\sqrt{3}$. The Laplace transforms can be inverted exactly in both cases to find $\langle J_d^3(t) \rangle$ and $\langle J_d^4(t) \rangle$. However, the expressions are rather long and complicated, and as we are interested in the approach to the Gaussian, it suffices to provide the expression in the long-time limit only. The third moment is proportional to $(r_1 - r_2)$, and grows as t^3 at large times,

$$\begin{aligned} \langle J_d^3(t) \rangle &= (r_1 - r_2) \left[\frac{(r_1 - r_2)^2 t^3}{8r^{\frac{3}{2}}} + \frac{3t^2}{16\pi r^{\frac{5}{2}}} \left(4b\pi r^{\frac{5}{2}} + 8r^2 - 3\pi(r_1 - r_2)^2 \right) \right. \\ &\quad \left. + \frac{t}{96\pi r^{\frac{7}{2}}} \left(135\pi(r_1 - r_2)^2 - 72r^2(3 + b(\pi - 4)\sqrt{r}) + \pi c_1 r \right) \right] + \mathcal{O}(1). \end{aligned} \quad (46)$$

The fourth moment grows as t^4 for large t ,

$$\begin{aligned} \langle J_d(t)^4 \rangle &= \frac{(r_1 - r_2)^4 t^4}{16r^2} + \frac{(r_1 - r_2)^2 t^3}{4\pi r^3} \left[6r^2 + 3b\pi r^{5/2} - 2\pi(r_1 - r_2)^2 \right] \\ &\quad + t^2 \left[3 \left(\frac{1}{\pi} + \frac{b\sqrt{r}}{2} \right)^2 + \frac{9(r_1 - r_2)^4}{4r^4} \right. \\ &\quad \left. - (r_1 - r_2)^2 \left(\frac{6}{\pi r^2} - \frac{3b(16 - 7\pi)}{8\pi r^{\frac{3}{2}}} + \frac{c_1}{6r} \right) \right] + \mathcal{O}(t). \end{aligned} \quad (47)$$

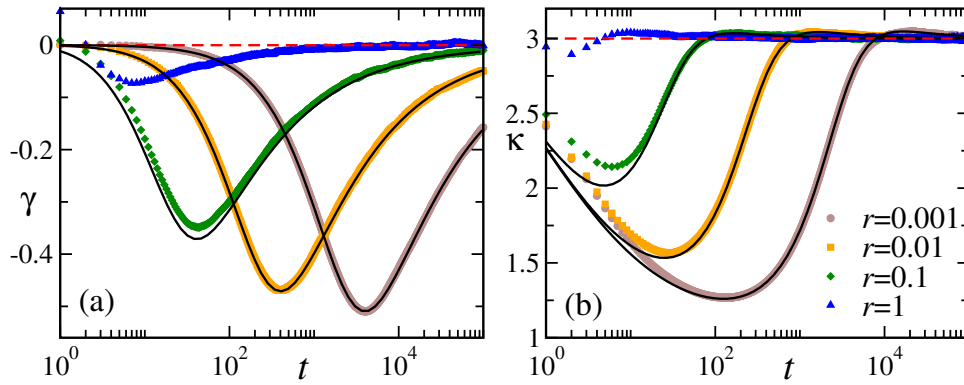


Figure 7. Skewness γ (a) and kurtosis κ (b) as a function of time t for different values of r and $\alpha = 0.8$. The symbols correspond to the data from the numerical simulations and the black solid lines correspond to the analytical predictions (see Eqs. (46) and (47)). The system size used for the numerical simulations is $L = 1000$.

From the above expressions it is straightforward to see that the third central moment $\langle (J_d - \langle J_d \rangle)^3 \rangle \sim t$ at long-times. Hence, clearly, the skewness γ vanishes as $\sim 1/\sqrt{t}$, indicating that the current distribution becomes symmetric at late times. The exact time-dependent γ can be evaluated using Eqs. (37), (39), (42) (46). This is shown in Fig. 7(a) where the analytical prediction is compared to the data from numerical simulation. Clearly, γ vanishes for $t \gg r^{-1}$, whereas in the regime $1 \ll t \ll r^{-1}$ it has a negative value indicating an extended tail towards smaller values of J_d .

The kurtosis κ can also be calculated using the above equations. Figure 7(b) compares the analytical prediction of κ with the same obtained from numerical simulations for different values of r . As expected, the two agree very well for $t \gg 1$. The figure shows that, starting from zero, the kurtosis first decreases, reaches a minimum and then increases and becomes larger than 3 for a brief regime before approaching $\kappa = 3$ for large times $t \gg r^{-1}$. While the limit $\kappa = 3$ signifies the Gaussian nature of $P(J_d, t)$ at large times, $\kappa < 3$ at short-times indicates a sharply peaked distribution compared to a Gaussian one. To understand the approach to the Gaussian limit, we calculate the limiting behaviour of κ using the expressions for the moments,

$$\lim_{t \rightarrow \infty} \kappa_3 = 3 + \frac{A}{t}, \quad (48)$$

where A is a non-zero constant which depends on r_1, r_2 . Similar to the skewness, κ also approaches the Gaussian limit in an algebraic manner, albeit with a larger exponent -1 .

5. Zero-current state

A special scenario emerges when the two resetting rates are equal, *i.e.*, $r_1 = r_2 = \frac{r}{2}$. In this case, the resettings to \mathcal{C}_1 and \mathcal{C}_2 occur equally frequently, and consequently, the average density profile becomes flat in the stationary state and there is no diffusive

particle current flowing through the system. This is reminiscent of the equilibrium SEP on a periodic lattice, which also has these two features. However, in the presence of the dichotomous resetting, there is no detailed balance, and the system remains far away from equilibrium. It is then interesting to ask how one can characterize this zero-current nonequilibrium state and how is it different than the equilibrium state of ordinary SEP.

In this section we investigate this question and illustrate various aspects of the ZCS which distinguish it from the equilibrium SEP. Following the results presented in Sec. 4, we show that the temporal behaviour of the current fluctuations are different in the two cases. It also turns out that this ZCS shows non-trivial spatial and temporal correlations which are also very different than ordinary SEP. Moreover, we explore the response of this stationary ZCS to an external perturbation and show that the susceptibility in this case is drastically different from the same in the equilibrium SEP.

5.1. Current Fluctuations

The first significant difference between the equilibrium SEP and the ZCS in the presence of dichotomous resetting shows up in the fluctuation of the diffusive current. The temporal behaviour of the equilibrium fluctuations of the current has been studied in Ref. [36]. This corresponds to the case where the initial densities in the left and right half of the system are equal. Adapting their result to our case ($\rho = 1/2$) we have, in the long time limit,

$$\begin{aligned}\langle J_0^2(t) \rangle &\simeq \frac{1}{2} \sqrt{\frac{t}{\pi}}, \\ \langle J_0^4(t) \rangle &\simeq \frac{3t}{4\pi} + \frac{1}{8} \sqrt{\frac{t}{\pi}} (4 - 3\sqrt{2}),\end{aligned}\tag{49}$$

while, of course, the odd moments vanish. Moreover, the distribution of the current $J_0(t)$ becomes Gaussian at long-times; the approach to the Gaussian is characterized by an algebraic decay of the kurtosis at long times,

$$\lim_{t \rightarrow \infty} \kappa = 3 - (3 - 2\sqrt{2}) \sqrt{\frac{\pi}{2t}} + O\left(\frac{1}{t}\right).\tag{50}$$

For the ZCS, the moments of the diffusive current can be obtained by putting $r_1 = r_2$ in Eqs. (39) and (47) and we have, in the long time limit,

$$\begin{aligned}\langle J_d^2(t) \rangle &\simeq t \left(\frac{1}{\pi} + \frac{b\sqrt{r}}{2} \right), \\ \langle J_d^4(t) \rangle &\simeq 3t^2 \left(\frac{1}{\pi} + \frac{b\sqrt{r}}{2} \right)^2.\end{aligned}\tag{51}$$

Clearly, the fluctuations grow much faster compared to equilibrium case. Note that, the moments grow slower compared to the case $r_1 \neq r_2$ where $\langle J_d(t)^2 \rangle \sim t^2$ and $\langle J_d(t)^4 \rangle \sim t^4$. All the odd moments vanish, of course, and the skewness remains zero at all times. This is expected, as we are starting from a symmetric initial condition and $r_1 = r_2$ does not introduce any directional bias. Kurtosis, on the other hand, approaches the Gaussian

value 3 in the long time limit as t^{-1} ; see Eq. (48). Hence, the approach to a Gaussian distribution for the ZCS is much faster compared to the equilibrium case.

5.2. Configuration weights

As mentioned already, the ZCS is characterized by a flat stationary profile. However, the weights of different configurations which contribute to this flat profile need not be same. Let us recall that, for ordinary SEP on a periodic lattice, each configuration becomes equally likely in the equilibrium state. In presence of the dichotomous resetting with equal rates $r_1 = r_2$, the stationary probability of any configuration \mathcal{C} is obtained by taking the $t \rightarrow \infty$ limit in Eq. (4),

$$\mathcal{P}_{st}(\mathcal{C}) = \frac{r}{2} \int_0^\infty ds e^{-rs} \left[\mathcal{P}_0(\mathcal{C}, s | \mathcal{C}_1, 0) + \mathcal{P}_0(\mathcal{C}, s | \mathcal{C}_2, 0) \right], \quad (52)$$

where \mathcal{P}_0 denotes the configuration probabilities in the absence of resetting. For a large resetting rate r , the integration is dominated by the contribution from $s \ll r^{-1}$, and hence $\mathcal{P}_{st}(\mathcal{C})$ will be large for those configurations \mathcal{C} for which either $\mathcal{P}_0(\mathcal{C}, s | \mathcal{C}_1, 0)$ or $\mathcal{P}_0(\mathcal{C}, s | \mathcal{C}_2, 0)$ is large for small s , *i.e.*, configurations which are ‘dynamically close’ to \mathcal{C}_1 and \mathcal{C}_2 . On the other hand, for smaller values of r , the integration is dominated by large values of s , and $\mathcal{P}_{st}(\mathcal{C})$ would have significant contributions for configurations ‘far’ from \mathcal{C}_1 and \mathcal{C}_2 .

To illustrate this point we take the simplest example of a lattice of size $L = 4$ and $L/2 = 2$ particles. In this case, there are 6 possible configurations including the resetting configurations $\mathcal{C}_1 = 1100$ and $\mathcal{C}_2 = 0011$. The stationary weights of the configurations can be calculated exactly, and yields, $\mathcal{P}_{st}(\mathcal{C}_1) = \mathcal{P}_{st}(\mathcal{C}_2) = \frac{r(r+6)+4}{2(r+2)(r+6)}$. Moreover, $\mathcal{P}_{st}(1010) = \mathcal{P}_{st}(0101) = \frac{1}{r+6}$ and $\mathcal{P}_{st}(1001) = \mathcal{P}_{st}(0110) = \frac{2}{(r+2)(r+6)}$. Of course, when $r = 0$, all the six configurations occur with equal weight. For any non-zero r the resetting configurations \mathcal{C}_1 and \mathcal{C}_2 have the highest stationary probability. For large values of r , the weight of the configurations 1010 and 0101, which can be reached from \mathcal{C}_1 or \mathcal{C}_2 by one hop (*i.e.*, dynamically close) vary as $1/r$ where as the weight of the configurations 1001 and 0110 (which are further away from the resetting configuration) decay as $1/r^2$. On the other hand, for small r all the configurations have comparable, although different, stationary weights.

5.3. Spatial correlations

It is interesting to investigate the spatial correlation of the SEP in the presence of the dichotomous resetting. Ordinary SEP, in the limit of thermodynamically large system size, has a product measure stationary state, so that the connected correlations vanish. In the presence of resetting, however, one can expect non-trivial spatial correlations, even for $r_1 = r_2$. In this section we explore the behaviour of the two point correlation $C_{x,y} = \langle s_x s_y \rangle$ in the presence of the dichotomous resetting.

For ordinary SEP, in equilibrium, all the configurations are equally likely. In particular, for a half-filled system of size L , each configuration has a probability $L^{-1} C_{L/2}$ to

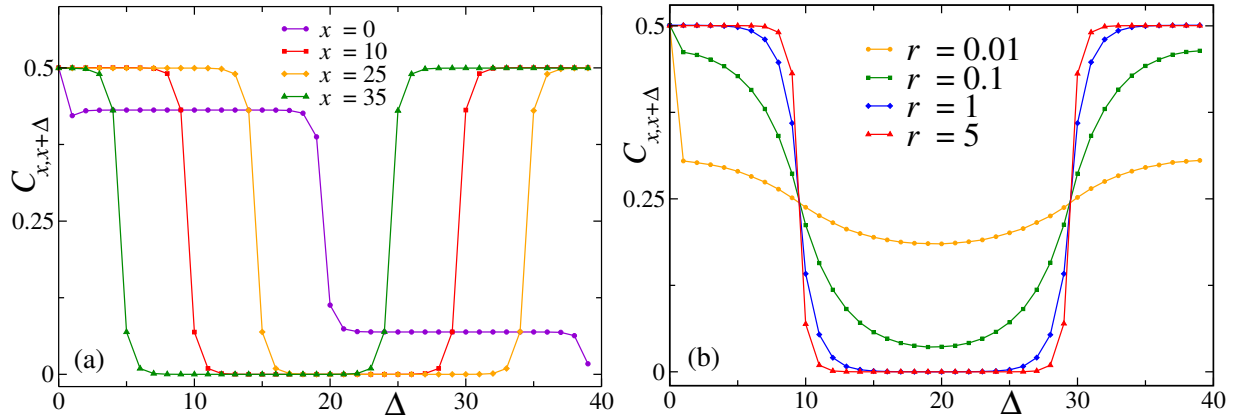


Figure 8. Plot of the two-point correlation $C_{x,x+\Delta}$ as a function of Δ for (a) a fixed (large) value of $r = 5$ and different values of x and (b) for fixed $x = 10$ and different values of r . The system size $L = 40$ here.

occur in the stationary (equilibrium) state. Correspondingly, the stationary two-point correlation for any finite system size L is given by,

$$C_{x,y} = \frac{(L-2)}{4(L-1)}, \quad (53)$$

which is independent of x and y and converges to $\rho^2 = 1/4$ for a thermodynamically large system.

In the presence of the resetting, it is straightforward to write a renewal equation for $C_{x,y}(t) = \sum_{\mathcal{C}} s_x(t)s_y(t)\mathcal{P}(\mathcal{C}, t|\mathcal{C}_0, 0)$ using Eq. (4). We are particularly interested in the case $r_1 = r_2$ and for the stationary correlation which is obtained by taking the limit $t \rightarrow \infty$,

$$C_{x,y} = \frac{r}{2} \int_0^\infty ds e^{-rs} [\langle s_x(s)s_y(s) \rangle_0^1 + \langle s_x(s)s_y(s) \rangle_0^2], \quad (54)$$

where $\langle s_x(s)s_y(s) \rangle_0^i$ denotes the spatial correlation in the absence of resetting, starting from the configuration $\mathcal{C}_i, i = 1, 2$. Unfortunately, it is hard to calculate the spatial correlations starting from the strongly inhomogeneous configurations \mathcal{C}_1 and \mathcal{C}_2 and hence we cannot get any analytical expression for $C_{x,y}$. However, we can get a qualitative idea about the same for the limiting case of large values of r .

For large $r \gg 1$, the integral in Eq. (54) is dominated by the contributions from small values of $s \ll r^{-1}$. In particular, starting from \mathcal{C}_1 and \mathcal{C}_2 , for sites x, y away from the boundaries between the two halves, s_x and s_y evolves very slowly, and as a first approximation we can use the values at time $s = 0$ to write,

$$\begin{aligned} C_{x,y} &\simeq \frac{1}{2} [\langle s_x(0)s_y(0) \rangle_0^1 + \langle s_x(0)s_y(0) \rangle_0^2] \\ &= \begin{cases} \frac{1}{2} & \text{if } 0 < x, y < \frac{L}{2}, \text{ or } \frac{L}{2} < x, y < L \\ 0 & \text{otherwise.} \end{cases} \end{aligned} \quad (55)$$

Figure 8(a) shows a plot of $C_{x,x+\Delta}$ as a function of Δ obtained from numerical simulations for different values of x for a fixed (large) value of $r = 5$. Clearly, for

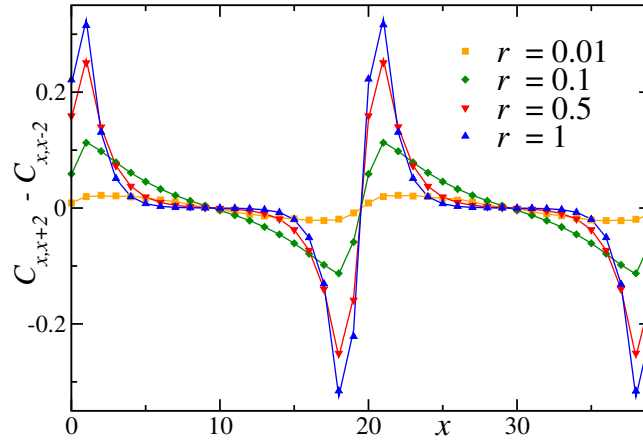


Figure 9. Spatial correlation in the stationary state: Comparison of $C_{x,x+2} - C_{x,x-2}$ (symbols) and $(r+2)[C_{x,x+1} - C_{x,x-1}] + \frac{r}{2}(\delta_{x,\frac{L}{2}-1} - \delta_{x,0} + \delta_{x,L-1} - \delta_{x,\frac{L}{2}})$ (solid lines) as a function of x for different values of r . The data is obtained from numerical simulations using a lattice of size $L = 40$.

$x > 0$, Eq. (55) provides a reasonably well prediction. On the other hand, for $r \rightarrow 0$, we expect that $C_{x,y} \rightarrow \frac{1}{4}$, the equilibrium value, independent of x, y .

The non-trivial nature of the spatial correlation for finite values of r is shown in Fig. 8(b) where $C_{x,x+\Delta}$, measured from numerical simulations, is plotted for different values of r . As r decreases the correlation between the two halves increases. To gain more information about the behaviour of C_{xy} for intermediate values of r we adopt a different approach. From the master equation (2), multiplying both sides of Eq. (2) by $s_x s_y$ and summing over all configurations \mathcal{C} we get the time-evolution equation for $C_{x,y}$. For $r_1 = r_2 = \frac{r}{2}$, this equation reads,

$$\begin{aligned} \frac{d}{dt} C_{x,y} = & C_{x,y+1} + C_{x,y-1} + C_{x+1,y} + C_{x-1,y} - (r+4)C_{x,y} + \frac{r}{2} \sum_{\mathcal{C}} s_x s_y (\delta_{\mathcal{C},c_1} + \delta_{\mathcal{C},c_2}) \\ & + \delta_{x+1,y} (2C_{x,y} - C_{x,y-1} - C_{x+1,y}) + \delta_{x-1,y} (2C_{x,y} - C_{x,y+1} - C_{x-1,y}). \end{aligned} \quad (56)$$

In the stationary state the left hand side vanishes, yielding a relation between C_{xy} at different spatial points,

$$\begin{aligned} C_{x,y+1} + C_{x,y-1} + C_{x+1,y} + C_{x-1,y} = & (r+4)C_{x,y} - \frac{r}{2} \sum_{\mathcal{C}} s_x s_y (\delta_{\mathcal{C},c_1} + \delta_{\mathcal{C},c_2}) \\ & - \delta_{x+1,y} (2C_{x,y} - C_{x,y-1} - C_{x+1,y}) - \delta_{x-1,y} (2C_{x,y} - C_{x,y+1} - C_{x-1,y}). \end{aligned} \quad (57)$$

While still not solvable exactly, this equation provides a simple relation between nearest neighbour and next nearest neighbour correlations. Substituting $y = x+1$ and $y = x-1$ in Eq. (57), we have, respectively,

$$C_{x,x+2} + C_{x-1,x+1} = (2+r)C_{x,x+1} - \frac{r}{2} \sum_{\mathcal{C}} s_x s_{x+1} (\delta_{\mathcal{C},c_1} + \delta_{\mathcal{C},c_2}), \quad (58)$$

$$C_{x,x-2} + C_{x-1,x+1} = (2+r)C_{x,x-1} - \frac{r}{2} \sum_{\mathcal{C}} s_x s_{x-1} (\delta_{\mathcal{C},c_1} + \delta_{\mathcal{C},c_2}) \quad (59)$$

for any value of x . Subtracting Eq. (59) from Eq. (58), we get,

$$\begin{aligned} C_{x,x+2} - C_{x,x-2} &= (2+r)(C_{x,x+1} - C_{x,x-1}) - \frac{r}{2} \sum_{\mathcal{C}} s_x(s_{x+1} - s_{x-1})(\delta_{\mathcal{C},\mathcal{C}_1} + \delta_{\mathcal{C},\mathcal{C}_2}) \\ &= (2+r)[C_{x,x+1} - C_{x,x-1}] + \frac{r}{2}(\delta_{\frac{L}{2}-1,x} - \delta_{0,x} + \delta_{L-1,x} - \delta_{\frac{L}{2},x}), \end{aligned} \quad (60)$$

where, in the last step, we have used the fact that the terms containing the $\delta_{\mathcal{C},\mathcal{C}_1}$ and $\delta_{\mathcal{C},\mathcal{C}_2}$ are non-zero only for four lattice sites, namely, $x = 0, \frac{L}{2} - 1, \frac{L}{2}$, and $x = L - 1$. This relation provides a way of directly demonstrating the non-trivial correlation induced by the presence of resetting. For Ordinary SEP, the quantity $(C_{x,x+2} - C_{x,x-2})$ vanishes in stationary state for all values of x , even for a finite lattice [see Eq. (53)]. On the other hand, Eq. (60) predicts a non-trivial r -dependent value for the ZCS.

We use numerical simulations to illustrate this non-trivial spatial correlation. Figure 9 shows a plot of $C_{x,x+2} - C_{x,x-2}$, measured directly (symbols), along with the right hand side of Eq. (60) (solid lines) as a function of x . The curves become more and more inhomogeneous, particularly near the boundaries $x = 0$ and $x = L/2$ between the two halves of the lattice, as the resetting rate r is increased indicating strong spatial correlation in the system. It is also consistent with the directly measured $C_{x,y}$ [see Fig. 8(a)] which shows a big jump near the boundaries $x = 0, L/2$ and hence resulting in a significant change in the difference also. Note that the difference also increases with r , in agreement with Eq. (60).

5.4. Temporal correlations

The presence of stochastic resetting is expected to affect the temporal correlations of the system as it introduces additional time-scales. In this section we investigate the behaviour of the density auto-correlation in the ZCS. In particular, we focus on the two-point auto-correlation at site x ,

$$\mathcal{G}(t, t + \tau) \equiv \langle s_x(t) s_x(t + \tau) \rangle = \sum_{\mathcal{C}, \mathcal{C}'} s_x(t + \tau) s_x(t) \mathcal{P}(\mathcal{C}', t + \tau | \mathcal{C}, t) \mathcal{P}(\mathcal{C}, t | \mathcal{C}_0, 0). \quad (61)$$

In the stationary state, $\mathcal{G}(t, t + \tau)$ is expected to depend only on τ .

In the absence of resetting, the stationary (*i.e.*, equilibrium) correlation $\mathcal{G}_0(\tau)$ can be calculated explicitly (see Appendix A) and for $\rho = \frac{1}{2}$ it turns out to be,

$$\mathcal{G}_0(\tau) = \frac{1}{4}[e^{-2\tau} I_0(2\tau) + 1]. \quad (62)$$

In the limit $\tau \rightarrow \infty$, $s_x(t)$ and $s_x(t + \tau)$ decorrelate and the auto-correlation saturates to $\rho^2 = \frac{1}{4}$. The approach to this value can be obtained from the above equation, and turns out to be algebraic in nature [35],

$$\tilde{\mathcal{G}}_0(\tau) \equiv \mathcal{G}_0(\tau) - \frac{1}{4} = \frac{1}{8\sqrt{\pi\tau}} + \mathcal{O}(\tau^{-1}). \quad (63)$$

To understand the effect of the resetting on the density auto-correlation, let us first recall that, for any $t > t'$, the corresponding conditional probability $\mathcal{P}(\mathcal{C}', t' | \mathcal{C}, t)$ satisfies

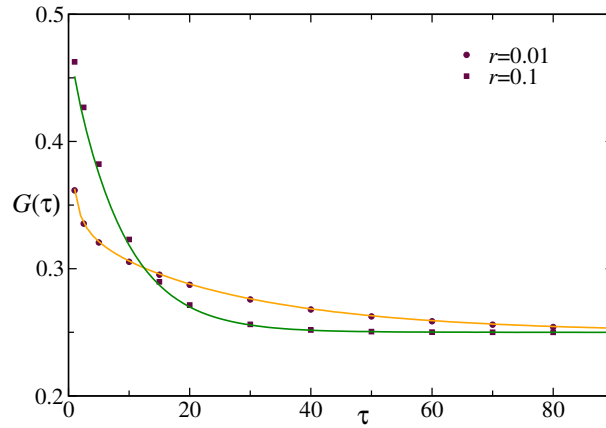


Figure 10. Numerical verification of Eq. (67) for two different values of r . The solid line represents left hand side of Eq. (67), while the dots represent the right hand side of the same equation.

a renewal equation (see Eq. (4)),

$$\mathcal{P}(\mathcal{C}, t | \mathcal{C}', t') = e^{-r(t-t')} \mathcal{P}_0(\mathcal{C}, t | \mathcal{C}', t') + \frac{r}{2} \int_0^{t-t'} ds e^{-rs} [\mathcal{P}_0(\mathcal{C}, s | \mathcal{C}_1, 0) + \mathcal{P}_0(\mathcal{C}, s | \mathcal{C}_2, 0)]. \quad (64)$$

Note that here we have restricted to the case $r_1 = r_2 = \frac{r}{2}$. Using Eq. (64) in Eq. (61) and performing the sums over the configurations we get,

$$\begin{aligned} \mathcal{G}(t, t + \tau) &= e^{-r(t+\tau)} \mathcal{G}_0(t, t + \tau) + \frac{r}{2} e^{-r\tau} \int_0^t ds e^{-rs} [\mathcal{G}_0^1(s, s + \tau) + \mathcal{G}_0^2(s, s + \tau)] \\ &\quad + \frac{r}{2} e^{-rt} \rho_0(x, t) \int_0^\tau ds e^{-rs} [\rho_0^1(x, s) + \rho_0^2(x, s)] \\ &\quad + \frac{r^2}{4} \int_0^\tau ds e^{-rs} [\rho_0^1(x, s) + \rho_0^2(x, s)] \int_0^t ds' e^{-rs'} [\rho_0^1(x, s') + \rho_0^2(x, s')], \end{aligned} \quad (65)$$

where $\mathcal{G}_0^i(t, t') = \langle s_x(t) s_x(t') \rangle_0$ denotes the auto-correlation in the absence of resetting starting from configuration \mathcal{C}_i and $\mathcal{G}_0(t, t')$ denotes the same starting from \mathcal{C}_1 and \mathcal{C}_2 with equal probability (which is our chosen initial condition). Similarly, $\rho_0(x, t)$ denotes the average density at site x at time t , starting from this chosen initial condition while $\rho_0^i(x, t) = \sum_{\mathcal{C}} s_x \mathcal{P}_0(\mathcal{C}, s | \mathcal{C}_i, 0)$ denotes the density starting from configuration \mathcal{C}_i , in the absence of resetting. Now, using the results of Sec. 3, it is easy to see that, $\rho_0^1(x, t) + \rho_0^2(x, t) = 1$ at any time t . Moreover, for our choice of initial condition (\mathcal{C}_1 and \mathcal{C}_2 with equal probability) $\rho_0(x, t) = 1/2$. Using these in Eq. (65) we get a renewal equation for $\mathcal{G}(t, t + \tau)$,

$$\begin{aligned} \mathcal{G}(t, t + \tau) &= e^{-r(t+\tau)} \mathcal{G}_0^0(t, t + \tau) + \frac{r}{2} e^{-r\tau} \int_0^t ds e^{-rs} [\mathcal{G}_0^1(s, s + \tau) + \mathcal{G}_0^2(s, s + \tau)] \\ &\quad + \frac{1}{4} (1 - e^{-r\tau}). \end{aligned} \quad (66)$$

In particular, in the stationary state $t \rightarrow \infty$, the auto-correlation depends on τ only,

$$\mathcal{G}(\tau) = \frac{r}{2} e^{-r\tau} \int_0^\infty ds e^{-rs} [\mathcal{G}_0^1(s, s + \tau) + \mathcal{G}_0^2(s, s + \tau)] + \frac{1}{4} (1 - e^{-r\tau}). \quad (67)$$

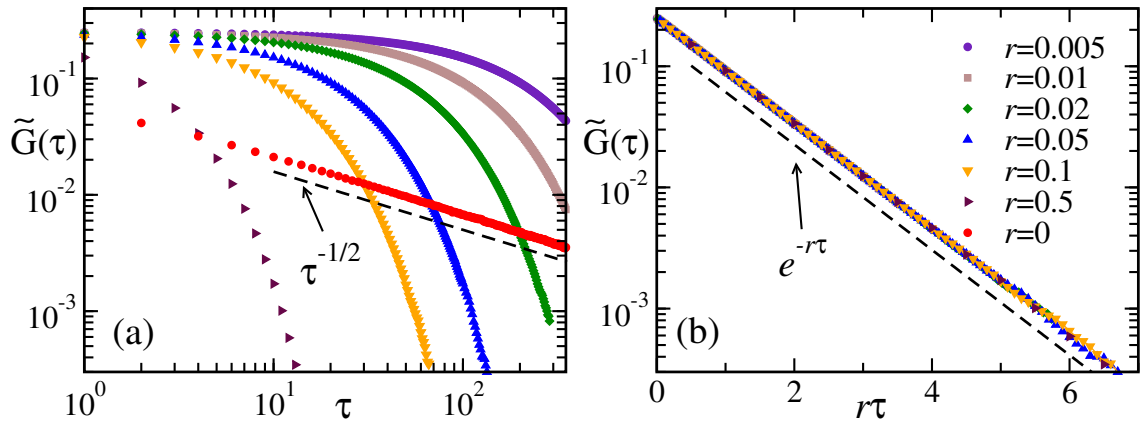


Figure 11. Figure (a) shows the graph for different values of r . We can see the crossover with the $r = 0$ case. (b) shows the same plot but as a function of scaled variable $r\tau$.

To verify this relation, using numerical simulations we measure $\mathcal{G}_0^1(s, s + \tau)$ and $\mathcal{G}_0^2(s, s + \tau)$ as a function of s , for different values of τ , in the absence of resetting. Then performing the integration over s numerically, we can compute the right hand side of Eq. (67). The data obtained thus are shown as the symbols in Fig. (10) for two different values of r . On the other hand, we also measure the stationary correlation $\mathcal{G}(\tau)$ in the presence of resetting directly which are shown as the black curves in the same figure. Clearly, the two measurements agree perfectly which verifies Eq. (67).

We can make further progress for small values of r . In this case the integral in Eq. (67) is dominated by large values of s . In this regime $\mathcal{G}_0^i(s, s + \tau)$ is expected to become independent of s ; as a first approximation we can use the stationary correlation $\mathcal{G}_0(\tau)$ given by Eq. (63). Then we get, from Eq. (67),

$$\mathcal{G}(\tau) \simeq e^{-r\tau} \left[\mathcal{G}_0(\tau) - \frac{1}{4} \right] + \frac{1}{4} = \frac{1}{4} [e^{-(r+2)\tau} I_0(2\tau) + 1]. \quad (68)$$

Using the asymptotic behaviour of the Bessel function it is easy to see that the connected correlation $\tilde{\mathcal{G}}(\tau)$ is expected to decay exponentially for large τ . This is shown in Fig. 11(a) where $\tilde{\mathcal{G}}(\tau)$ for different values of r , obtained from numerical simulations, are plotted as a function of τ . For easy reference we have also included the data for $r = 0$ which shows the $\tau^{-1/2}$ decay. Figure 11(b) shows the data for non-zero r plotted as a function of $r\tau$ which show a perfect collapse according to the predicted exponential decay.

This exponential temporal correlation is a typical feature of systems with stochastic resetting and originates from the fact that in the presence of resetting, the configurations are correlated only when they occur between two consecutive resetting epochs. Similar results have been observed in the context of single particle resetting with one rate in Ref. [39]. For our present case of SEP with dichotomous resetting we see that while the resetting creates strong spatial correlations, it effectively erases the non-trivial temporal correlation present in ordinary SEP, replacing it with a faster, exponential decay which

depends only on the resetting rate r .

5.5. Response to perturbation

How a system responds to an external perturbation plays an important role in characterizing the properties of the system. For a small perturbation around equilibrium, the response is predicted by the famous fluctuation-dissipation theorem (FDT) which gives an explicit form for the susceptibility in terms of equilibrium correlations [40]. For systems away from equilibrium, the linear response formula is different, notably, with the addition of a ‘frenetic’ contribution [41].

To further characterize the zero-current state for $r_1 = r_2$, and illustrate its nonequilibrium nature we investigate the response of the system to an external perturbation, and compare it with the same for equilibrium SEP. In the following we consider one of the simplest possible perturbations, namely, a biasing field ε across the central bond. This is implemented by a change in the hop rates *across the central bond*,

$$10 \xrightleftharpoons[q]{p} 01, \quad (69)$$

where $p/q = e^\varepsilon$, consistent with local detailed balance [42]. The hop rate for all the other bonds remains unchanged.

This bias generates a non-zero diffusive current, for both equilibrium SEP and the zero-current nonequilibrium state. For a small biasing field, the average current generated $\langle J_d(t) \rangle_\varepsilon$ is expected to be proportional to the field ε in both the cases with a susceptibility $\chi = \langle J_d(t) \rangle_\varepsilon / \varepsilon$ which depends on the fluctuations in the unperturbed state. In the equilibrium case, the response is given by the Kubo formula, which predicts that the susceptibility is proportional to the variance of the current in absence of the perturbation,

$$\chi_{\text{eq}} = \frac{1}{2} \langle J_d^2 \rangle_0 \equiv \langle J_0^2 \rangle. \quad (70)$$

where $\langle J_0^2 \rangle$ is the variance in the equilibrium state, *i.e.*, both in the absence of the resetting and the perturbation, given by Eq. (49). From the above equation and Eq. (49), it is clear that the average current generated due to the perturbation to ordinary SEP grows as \sqrt{t} with time.

To predict the response of the ZCS to the perturbation one has to take recourse to the nonequilibrium response theory [41]. Using path integral formalism, the linear response can be expressed in terms of correlations in absence of the perturbation,

$$\chi_r = \frac{1}{2} \langle \mathcal{S}(\omega) J_d \rangle - \langle \mathcal{D}(\omega) J_d \rangle. \quad (71)$$

Here $\mathcal{S}(\omega)$ and $\mathcal{D}(\omega)$ respectively denote the *excess* entropy and dynamical activity generated by the perturbation along the trajectory ω during the interval $[0, t]$; the correlations are calculated by averaging over all possible trajectories in the zero-current state, *i.e.*, in the presence of the resetting but in the absence of the perturbations. The path dependent quantities \mathcal{S} and \mathcal{D} are the time-antisymmetric and time-symmetric

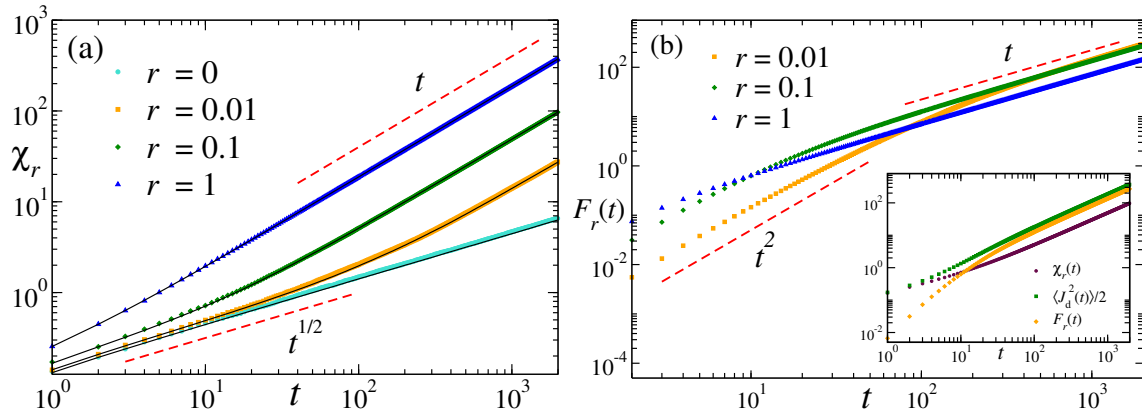


Figure 12. Linear response in ZCS: (a) Plot of the nonequilibrium susceptibility χ_r vs t for different values of r . The symbols correspond to the predicted response Eq. (74) measured in the unperturbed system, while the solid lines corresponds to direct measurement of susceptibility in the presence of a perturbation of strength $\varepsilon = 0.1$. For $r > 0$, χ_r grows $\sim t$ at large times while for $r = 0$ it grows as \sqrt{t} . (b) Plot of the frenetic component $F_r(t) = \frac{1}{2}(\langle t_{10} J_d \rangle - \langle t_{01} J_d \rangle)$ which shows a crossover from a t^2 behaviour at short-times to a linear growth at late times. The inset shows the entropic and frenetic components along with the total χ_r for a fixed $r = 0.1$. All the simulations are done on a lattice of size $L = 1000$.

parts of the path-action calculated with respect to the unperturbed path weights and can be explicitly computed for any stochastic process given the perturbation protocol. For detailed prescription of how to compute these quantities see Refs. [41, 43]. Here we just give the expressions for the particular perturbation under consideration. The excess entropy is independent of the specific form of p and q , and is given by,

$$\mathcal{S}(\omega) = J_d. \quad (72)$$

Hence, the first term in Eq. (71) is nothing but the Kubo-term, measuring the variance in the unperturbed state. On the other hand, the excess dynamical activity depends explicitly on p and q

$$\mathcal{D}(\omega) = -\frac{1}{2} \mathcal{N} \frac{d}{d\varepsilon} (\ln pq) \Big|_{\varepsilon=0} + \frac{dp}{d\varepsilon} \Big|_{\varepsilon=0} t_{10} + \frac{dq}{d\varepsilon} \Big|_{\varepsilon=0} t_{01}. \quad (73)$$

Here \mathcal{N} denotes the *total* number of jumps across the central bond (both towards right and left). Moreover, t_{01} (respectively, t_{10}) denotes the total time in $[0, t]$ during which the local configuration is 01 (respectively, 10) in the central bond, *i.e.*, $s_{\frac{L}{2}-1} = 0, s_{\frac{L}{2}} = 1$ (respectively, $s_{\frac{L}{2}-1} = 1, s_{\frac{L}{2}} = 0$).

To proceed further, we need to specify p and q . For the sake of simplicity, we consider $p = e^{\varepsilon/2}$ and $q = e^{-\varepsilon/2}$. Note that this formula depends crucially on the choice of p, q but for our purpose it suffices to consider this simple choice. In this case $pq = 1$ and Eq. (73) simplifies leading to the nonequilibrium susceptibility,

$$\chi_r(t) = \frac{1}{2} [\langle J_d^2(t) \rangle - \langle t_{10} J_d \rangle + \langle t_{01} J_d \rangle]. \quad (74)$$

The first term is nothing but the variance of the diffusive current in the presence of the dichotomous resetting which we have already calculated in Sec. 4 [see Eq. (39) with

$r_1 = r_2$]. The frenetic component $F_r(t) = \frac{1}{2}(\langle t_{10} J_d \rangle - \langle t_{01} J_d \rangle)$ involves correlation of the current with time-symmetric quantities t_{01} and t_{10} and we take recourse to numerical simulations to measure these. We also measure the susceptibility directly by applying the perturbation and calculating $\chi_r = \langle J_d \rangle_\varepsilon / \varepsilon$. Figure 12(a) compares the χ_r predicted by Eq. (74) (symbols) with the directly measured χ_r (solid lines) for different values of r . For $r > 0$, at late times, the susceptibility grows linearly with t which is drastically different than the $r = 0$ scenario, where the susceptibility $\sim \sqrt{t}$. Note that, at short-times $t \ll r^{-1}$, the system shows an equilibrium-like behaviour with $\chi_r \sim \sqrt{t}$.

It is interesting to look at the frenetic component $F_r(t)$ separately. Figure 12(b) shows plots of $F_r(t)$ for different values of r . At short-times $t \ll r^{-1}$ it shows a t^2 behaviour, and is thus negligible compared to the entropic component which $\sim \sqrt{t}$ in this regime [see Eq. (39) with $r_1 = r_2$]. Hence the total response in this regime is dominated by the entropic component only, which is expected, as at short-times the effect of resetting is not visible, and the system remains close to equilibrium. At late-times, $F_r(t)$ shows a $\sim t$ behaviour, similar to the entropic part and the total response also becomes linear. The inset in Fig. 12(b) shows the entropic and frenetic components along with the χ_r for a fixed r ; clearly, the negative contribution from the frenetic component reduces the slope of the total response.

To summarize, the study of the linear response in the ZCS shows two important features which distinguish it from equilibrium SEP. First, the same perturbation, namely, a small driving field gives rise to very different currents in the two cases – in presence of the resetting the current grows much faster. Secondly, the linear response has a frenetic contribution which competes with the traditional Kubo term and reduces the slope of the susceptibility (as a function of time).

6. Conclusions

In this article we have studied the behaviour of symmetric exclusion process in the presence of dichotomous stochastic resetting. The dichotomous resetting is implemented by resetting the system to either of the two specific configurations where all the particles are in the left (respectively, right) half of the system, with rates r_1 (respectively r_2). The presence of the dichotomous resetting leads to intriguing dynamical and stationary properties, which we have characterized. We have exactly calculated time-evolution of the density profile which remains inhomogeneous in the stationary state.

The primary quantity of interest is the diffusive particle current across the central bond. We show that for any $r_1 \neq r_2$ the current grows linearly with time, with a coefficient proportional to $(r_1 - r_2)$. In the long-time limit the distribution of the current converges to a Gaussian distribution, while at the short-time regime there are strong non-Gaussian fluctuations which we characterize via skewness and kurtosis. We demonstrate that both skewness and kurtosis approach the Gaussian limit with an algebraic decay in time.

A special scenario arises when $r_1 = r_2$. In this case, the system reaches a stationary

state where the density profile is uniform and there is no particle current flowing through the system. Nevertheless, the system stays far away from equilibrium and we characterize this zero current nonequilibrium state by computing the spatial and temporal density correlations. We show that while the presence of the resetting induces non-trivial spatial correlations, it also reduces the temporal correlations - instead of an algebraic temporal decay of the auto-correlation (which is seen for equilibrium SEP), we get an exponential decay in the presence of the resetting. Finally, we also study the response of the ZCS to a small perturbation and show that the response is linear in time instead of the \sqrt{t} behaviour expected in equilibrium.

We conclude with the final remark that the simple dichotomous resetting protocol leads to a more rich and complex behaviour compared to resetting with a single rate and it would be interesting to study the effect of such resetting protocols for single particle systems as well as more complicated interacting systems.

Acknowledgments

The authors thank Riddhipratim Basu, Aanjaneya Kumar and Christian Maes for helpful discussions. O. S. acknowledges the Inspire grant from DST, India and support from Raman Research Institute where he worked as a visiting student and where this work was carried out. U. B. acknowledges support from Science and Engineering Research Board, India under Ramanujan Fellowship (Grant No. SB/S2/RJN-077/2018).

Appendix A. Density auto-correlation for ordinary SEP

In this Section we briefly revisit the temporal auto-correlation of equilibrium SEP, *i.e.*, in the absence of resetting. In particular, we look at the density auto-correlation at site x ,

$$\mathcal{G}^0(t) = \langle s_x(0)s_x(t) \rangle = \langle s_x(t) | s_x = 1, t = 0 \rangle. \quad (\text{A.1})$$

Clearly, it is nothing but the density $\rho_x(t)$ at site x , averaged over all possible initial configurations with $s_x = 1$. For SEP without resetting, we know that, starting from any initial density profile $\phi_0(y)$, the density at time t is given by,

$$\rho_x(t) = \frac{1}{2} + \frac{1}{L} \left[\sum_{n=1}^{L-1} \tilde{\phi}_0(n) e^{-\lambda_n t} e^{-i \frac{2\pi n x}{L}} \right], \quad (\text{A.2})$$

where, $\tilde{\phi}_0(n)$ is the Fourier transform of $\phi_0(y)$. To compute the auto-correlation, we need the initial profile such that the density at site x is 1. In equilibrium, for a large system size L , this is given by,

$$\phi_0(y) = \begin{cases} 1 & \text{when } y = x \\ \rho & \text{when } y \neq x, \end{cases} \quad (\text{A.3})$$

where, ρ is the global particle density of the system. The corresponding Fourier transform is given by,

$$\begin{aligned}\tilde{\phi}_0(n) &= \sum_{y=0}^{L-1} e^{i\frac{2\pi ny}{L}} \phi_0(y) = e^{i\frac{2\pi nx}{L}} + \rho \sum_{y \neq x}^{L-1} e^{i\frac{2\pi ny}{L}} \\ &= (1 - \rho) e^{i\frac{2\pi nx}{L}}.\end{aligned}\tag{A.4}$$

Substituting Eq. (A.4) in Eq. (A.2), we get for $\rho = \frac{1}{2}$,

$$\rho_x(t) = \frac{1}{4} \left(1 + \frac{1}{L} \sum_{n=1}^{L-1} e^{-\lambda_n t} \right).\tag{A.5}$$

For large system size L , we can convert the summation to integral as done before in Eq. (17). We get,

$$\begin{aligned}\mathcal{G}^0(t) &= \frac{1}{4} + \frac{1}{8\pi} \int_0^{2\pi} dq e^{-\lambda_q t} \\ &= \frac{1}{4} [1 + e^{-2t} I_0(2t)],\end{aligned}\tag{A.6}$$

where I_0 is the modified Bessel function of the first kind. As expected, at large time $t \rightarrow \infty$, the correlation decays to $\rho^2 = \frac{1}{4}$. The approach to this stationary value can be obtained from the asymptotic behaviour of I_0 ,

$$\mathcal{G}^0(t) - \frac{1}{4} = \frac{1}{8\sqrt{\pi t}}.\tag{A.7}$$

which is quoted as Eq. (63) in Sec. (5.4) of the main text.

- [1] M. R. Evans, S. N. Majumdar, and G. Schehr, [arXiv:1910.07993](#).
- [2] M. R. Evans and S. N. Majumdar, *Phys. Rev. Lett.* **106**, 160601 (2011).
- [3] M. R. Evans and S. N. Majumdar, *J. Phys. A: Math. Theor.* **44**, 435001 (2011).
- [4] O. Tal-Friedman, A. Pal, A. Sekhon, S. Reuveni, and Y. Roichman, [arXiv:2003.03096](#).
- [5] M. R. Evans, S. N. Majumdar, and K. Mallick, *J. Phys. A: Math. Theor.* **46**, 185001 (2013).
- [6] J. Whitehouse, M. R. Evans, and S. N. Majumdar, *Phys. Rev. E* **87**, 022118 (2013).
- [7] M. R. Evans and S. N. Majumdar, *J. Phys. A: Math. Theor.* **47**, 285001 (2014).
- [8] V. Méndez and D. Campos, *Physical Review E* **93**, 022106 (2016).
- [9] A. Masó-Puigdellosas, D. Campos, and V. Méndez, *Physical Review E* **99**, 012141 (2019).
- [10] A. Pal, R. Chatterjee, S. Reuveni, and A. Kundu, *J. Phys. A* **52**, 264002 (2019).
- [11] A. Pal, *Phys. Rev. E* **91**, 012113 (2015).
- [12] S. Ahmad, I. Nayak, A. Bansal, A. Nandi, and D. Das, *Phys. Rev. E* **99**, 022130 (2019).
- [13] A. Chatterjee, C. Christou, and A. Schadschneider, *Phys. Rev. E* **97**, 062106 (2018).
- [14] A. Pal and V. V. Prasad, *Phys. Rev. E* **99**, 032123 (2019).
- [15] D. Gupta, *J. Stat. Mech.*, 033212 (2019).
- [16] D. Boyer and C. Solis-Salas, *Phys. Rev. Lett.* **112**, 240601 (2014).
- [17] S. N. Majumdar, S. Sabhapandit, and G. Schehr, *Phys. Rev. E* **92**, 052126 (2015).
- [18] A. Masó-Puigdellosas, D. Campos, and V. Méndez, *Front. Phys.* **7**, 112 (2019).
- [19] E. Roldán, S. Gupta, *Phys. Rev. E* **96**, 022130 (2017).
- [20] A. Pal, A. Kundu, and M. R. Evans, *J. Phys. A: Math. Theor.* **49**, 225001 (2016).
- [21] V. P. Shkilev, *Phys. Rev. E* **96**, 012126 (2017).
- [22] A. Nagar and S. Gupta, *Phys. Rev. E* **93**, 060102 (2016).
- [23] S. Eule and J. J. Metzger, *New J. Phys.* **18**, 033006 (2016).

- [24] A. S. Bodrova, A. V. Chechkin, I. M. Sokolov, Phys. Rev. E **100**, 012119 (2019).
- [25] M. R. Evans and S. N. Majumdar, J. Phys. A: Math. Theor. **52**, 01LT01 (2019).
- [26] A. Masó-Puigdellosas, D. Campos and V. Méndez, J. Stat. Mech., 033201 (2019).
- [27] A. Pal, Ł. Kuśmierz, and S. Reuveni, New J. Phys. **21**, 113024 (2019).
- [28] S. Gupta, S. N. Majumdar, and G. Schehr, Phys. Rev. Lett. **112**, 220601 (2014).
- [29] X. Durang, M. Henkel, and H. Park, J. Phys. A: Math. Theor. **47**, 045002 (2014).
- [30] U. Basu, A. Kundu, and A. Pal, Phys. Rev. E **100**, 032136 (2019).
- [31] P. Grange, [arXiv:1910.05991](#).
- [32] P. Grange, [arXiv:1912.06024](#).
- [33] M. Magoni, S. N. Majumdar, G. Schehr, [arXiv:2002.04867](#).
- [34] *Interacting Particle Systems*, T. Liggett, Springer-Verlag, Berlin (1985).
- [35] *Large Scale Dynamics of Interacting Particles*, H. Spohn, Springer-Verlag, Berlin (1991).
- [36] B. Derrida, A. Gerschenfeld, J. Stat. Phys. **136**, 1 (2009).
- [37] B. Derrida, B. Douçot, and P. E. Roche, J. Stat. Phys. **115**, 717 (2004).
- [38] NIST Digital Library of Mathematical Functions, F. W. J. Olver, A. B. Olde Daalhuis, D. W. Lozier, B. I. Schneider, R. F. Boisvert, C. W. Clark, B. R. Miller, B. V. Saunders, H. S. Cohl, and M. A. McClain, eds.
- [39] S. N. Majumdar and G. Oshanin, J. Phys. A: Math. Theor. **51**, 435001 (2018).
- [40] R. Kubo, Rep. Prog. Phys. **29**, 255 (1966).
- [41] M. Baiesi, C. Maes, and B. Wynants, Phys. Rev. Lett. **103**, 010602 (2009).
- [42] S. Katz, J. Lebowitz and H. Spohn, J. Stat. Phys. **34**, 497 (1984).
- [43] M. Baiesi and C. Maes, New J. Phys. **15**, 013004 (2013).